

**UNCLASSIFIED**

**AD**

**408 415**

---

**DEFENSE DOCUMENTATION CENTER**

FOR

**SCIENTIFIC AND TECHNICAL INFORMATION**

CAMERON STATION, ALEXANDRIA, VIRGINIA



**UNCLASSIFIED**

NOTICE: When government or other drawings, specifications or other data are used for any purpose other than in connection with a definitely related government procurement operation, the U. S. Government thereby incurs no responsibility, nor any obligation whatsoever; and the fact that the Government may have formulated, furnished, or in any way supplied the said drawings, specifications, or other data is not to be regarded by implication or otherwise as in any manner licensing the holder or any other person or corporation, or conveying any rights or permission to manufacture, use or sell any patented invention that may in any way be related thereto.

⑤ 741150

63-4-2

①

Scale = 1

RADC-TDR-63-199

April 1963

AD No. 408415

DDC FILE COPY

PHOTOELECTRIC MILLIMETER WAVE DETECTOR

Peter R. Bratt  
Peter P. Debye  
George F. Giggey  
Said Koozekanani

RAYTHEON COMPANY  
Research Division  
Spencer Laboratory  
Burlington, Massachusetts

S-553

Contract No. AF30(602)-2637

DDC  
JUL 12 1963  
TISIA A

Prepared for

Rome Air Development Center  
Research and Technology Division  
Air Force Systems Command  
United States Air Force  
Griffiss Air Force Base  
New York

408 415

#6.60

PATENT NOTICE: When Government drawings, specifications, or other data are used for any purpose other than in connection with a definitely related Government procurement operation, the United States Government thereby incurs no responsibility nor any obligation whatsoever and the fact that the Government may have formulated, furnished, or in any way supplied the said drawings, specifications or other data is not to be regarded by implication or otherwise as in any manner licensing the holder or any other person or corporation or conveying any rights or permission to manufacture, use, or sell any patented invention that may in any way be related thereto.

ASTIA NOTICE: Qualified requestors may obtain copies of this report from the ASTIA Document Service Center, Arlington Hall Station, Arlington 12, Virginia. ASTIA Services for the Department of Defense contractors are available through the "Field of Interest Register" on a "need-to-know" certified by the cognizant military agency of their project or contract.

(18) (19) RADC-TDR-63-199

(4) #1.60 (5) 741 150

(11) April 1963

(6) PHOTOELECTRIC MILLIMETER WAVE DETECTOR

(10) by Peter R. Bratt,  
Peter P. Debye,  
George F. Giggey, *and*  
Said Koozekanani.

RAYTHEON COMPANY  
Research Division  
Spencer Laboratory  
Burlington, Massachusetts

(14) *Revised* S-553

(12) 57 p.

(13) N/A

(20) 2L

(32) N/A

(15) Contract No. AF30(602)-2637

(16) Project No. 5578

(17) Task No. 557801

Prepared for

Rome Air Development Center  
Research and Technology Division  
Air Force Systems Command  
United States Air Force  
Griffiss Air Force Base  
New York

*79*

## FOREWORD

a. The objective of this contract was a study and investigation to determine the feasibility of developing a photoelectric detector for use in the millimeter and submillimeter wave region. The study was to include: magnetically induced energy gaps in semiconductors, frequency response, sensitivity and response time. The end items were to be a final report, and an experimental model of a photoelectric millimeter wave detector in accordance with the techniques developed under the study.

b. The approach taken by the Contractor to fulfill the requirements was scientifically sound. The feasibility of using photoconductive indium antimonide in a magnetic field and at temperatures of  $1^{\circ}$  to  $2^{\circ}$  K as a detector has been reported by E. H. Putley, in the Proc. Phys. Soc. (London) 76, 802 (1960).

(1) The operation of this type of detector is dependent upon the ability of incoming electromagnetic radiation to excite into conduction, bound electrons within a semiconducting material (i. e., the photoconductive effect). This is accomplished if the photon energy  $h\nu$  is equal to, or greater than, the ionization energy,  $\Delta\epsilon$  of an impurity atom within the semiconductor. This photoconductivity has been useful for the detection of infrared radiation using a material such as germanium. At millimeter wavelengths, however, the ionization energy must be extremely small, of the order of  $1/10$  that which can be obtained with impurities in germanium.

(2) Calculations have shown that donor atoms in the semiconductor indium antimonide would have the necessary small ionization energy. Low temperatures, of the order of  $4^{\circ}$ K or less, are necessary in order to overcome electron excitation due to thermal energy. Impurity band conduction tends to overshadow photoconductivity effects. The application of a magnetic field causes a narrowing of this impurity band and also a splitting of the impurity levels away from the conduction band.

(3) Hall effect and resistivity measurements were conducted on several samples. Theoretical analysis, and analytic assumptions were made in an effort to extrapolate from these measurements such meaningful data as Hall coefficient,

impurity concentration and mobility. Measurements were made versus temperature at various magnetic field intensities. Photoconductive response was also measured. Signal-to-noise ratio versus bias as a function of different magnetic field intensities were plotted and sensitivity (detectivity) of the detector was calculated. Interesting to note was the effect, at higher bias currents, of the decrease in sensitivity by the application of the increased magnetic field. This is directly in contrast to that reported by Putley. However, Putley's work was centered around the submillimeter range, and the measurements taken by Raytheon were at the longer (millimeter) wavelengths. It is expected that the results at Raytheon would be the same as Putley's at the submillimeter wavelengths.

c. The results of this contract have shown that a photoconductive detector can be fabricated, for millimeter wavelengths, that is comparable in sensitivity, and faster in response time, than can be incurred in present devices such as bolometers and other heat sensitive cells. The equivalent noise power, for a 1 CPS bandwidth, of the device delivered is about  $5 \times 10^{-12}$  watts at 4 millimeters wavelength. The results do indicate that further study is required, particularly to determine the effects of high magnetic field intensities with the higher biasing levels at the longer wavelengths.

d. The photoelectric detector developed on this contract has a particular application to the Air Force need for transmission line components to be used in future systems at these frequencies. The particular detector developed on this contract may also serve to aid in the evaluation of other types of components in the frequency range.

JOSEPH J. LO MASCOLO  
Project Engineer  
RADC, Griffiss AFB, N. Y.

## PHOTOELECTRIC MILLIMETER WAVE DETECTOR

### ABSTRACT

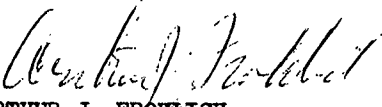
~~has been~~<sup>WAS</sup> The purpose of this program is a study and investigation of a photoconductive type of detector sensitive to radiation in the millimeter and sub-millimeter wave regions of the electromagnetic spectrum. The detector utilizes a magnetically-induced energy gap in indium antimonide and operates at temperatures of 4°K, or below. Although the main emphasis of the work ~~has been~~<sup>WERE</sup> directed toward the development of a practical operating device, some fundamental studies of the properties of indium antimonide at low temperatures and in a large magnetic field ~~have also been~~<sup>WERE</sup> carried out. A detector has been developed having the following properties:

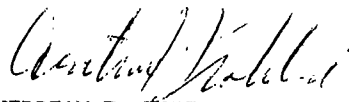
- a. A sensitive element mounted in an all metal double Dewar-type housing for convenient cooling with liquid helium,
- b. An integral superconducting solenoid to provide the necessary magnetic field,
- c. Fast response time, and
- d. High sensitivity to radiation in the wavelength range from below 0.1 mm to at least 8 mm. Typical detectivity at 4 mm is  $D^* (4 \text{ mm}, 1000, 1) = 1 \times 10^{11} \text{ cm cps}^{1/2}/\text{watt}$ . This corresponds to a minimum detectable energy (i. e. , noise equivalent power for 1 cps bandwidth) of  $5 \times 10^{-12} \text{ watts}$ .

Title of Report      RADC-TDR-63-199

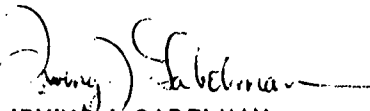
**PUBLICATION REVIEW**

This report has been reviewed and is approved.

Approved:   
ARTHUR J. FROHLICH  
Chief, Techniques Laboratory  
Directorate of Aerospace Surveillance & Control

Approved:   
WILLIAM T. POPE  
Acting Director  
Director of Aerospace  
Surveillance & Control

FOR THE COMMANDER:

  
IRVING J. GABELMAN  
Director of Advanced Studies

FINAL REPORT  
PHOTOELECTRIC MILLIMETER WAVE DETECTOR

TABLE OF CONTENTS

<u>Section</u>		<u>Page</u>
1.0	Introduction	1
2.0	The Detector Material	6
	2.1 Hall Effect Analysis	6
	2.2 Photoconductive Response	20
	2.3 Absorption Coefficient	32
3.0	The Sample Detector	35
	3.1 Package Requirements	35
	3.2 Operating Instructions	50
	References	

## PHOTOELECTRIC MILLIMETER WAVE DETECTOR

### 1.0 INTRODUCTION

Photoconductive detectors of electromagnetic radiation utilizing various semiconducting materials have proven their usefulness in the visible and infrared regions of the spectrum, and are finding numerous applications in various systems for both industrial and military purposes. They generally respond to a broad band of radiation wavelengths, are extremely sensitive, have fast response times, and are relatively easy to operate. Such detectors would be useful if they could also be made to operate in the millimeter and submillimeter wave region. Up until fairly recently, the only detector for this wavelength region was the thermal type of detector such as the bolometer, thermocouple or pneumatic cell. While these detectors are also broadband detectors, they are relatively slow in response and somewhat limited in sensitivity. A photoconductive type of detector for this wavelength region, therefore, has advantages which could lead to many new applications in military, research and industrial technologies.

The operation of the photoconductive type of detector depends on the existence of bound electrons (non-conducting) in a host material which can be excited into the free state (conducting) by supplying them with a certain amount of energy,  $\Delta\epsilon$ , through absorption of a quantum of electromagnetic radiation of frequency,  $\nu$ , such that  $h\nu \geq \Delta\epsilon$ , where  $h$  is Planck's constant. This is illustrated in Figure 1.

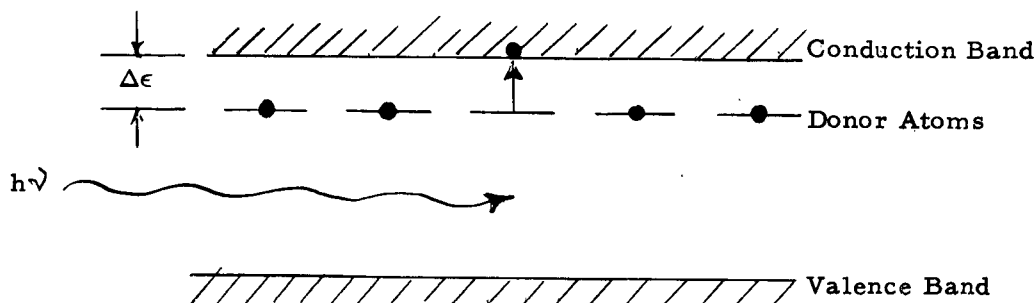


Figure 1 Ionization of Donor Impurity in a Semiconductor by a Quantum of Radiation. An electron is transferred from a bound state on the donor atom to a free state in the conduction band, thereby producing an increase in the conductivity.

For radiation with a frequency at 300 kMc (1 millimeter wavelength), the energy gap required is  $1.2 \times 10^{-3}$  eV. Because of such a small energy gap between the bound and free electron states, it is essential that this type of detector be cooled to very low temperatures, otherwise the thermal energy of the host crystal lattice would excite the electrons into the free state and no photoconductivity would be observed. Since the thermal energy of the crystal is of the order of  $kT$ , where  $k$  is the Boltzmann constant and  $T$  the absolute temperature, the amount of cooling necessary is dictated by the requirement that  $kT \ll \Delta\epsilon$ . Thus, with the energy gaps under consideration here, it is clear that temperatures of just a few degrees absolute are required.

Photoconductive detectors have been made utilizing germanium crystals containing impurity atoms such as antimony<sup>1</sup> and indium<sup>2</sup> to provide bound states from which electrons can be excited to the free state. However, the impurity ionization energy in this material is about .01 eV; thus, photoconductivity is observed only out to wavelengths of about 120 microns (.12 millimeters) in the infrared region. As noted above, an energy gap one-tenth of this value is required to extend the photoconductive response out to the millimeter region.

Calculations have shown that n-type InSb containing donor impurities such as selenium and tellurium would have an ionization energy gap of about  $7 \times 10^{-4}$  eV, and thus should exhibit photoconductivity out to 1800 microns (1.8 millimeters). However, on cooling such material to very low temperatures, no "freeze out" of free electrons into the bound states is observed<sup>3</sup>; hence, no photoconductivity is found. This effect is due to the interaction of neighboring impurity atoms with each other producing what is called an impurity band.<sup>4-6</sup> Motion of an electron within an impurity band is similar to the motion of a free electron in the conduction band except for differences in mobility between the two bands. In the case of n-type indium-antimonide, the impurity band apparently overlaps the conduction band so that no impurity ionization energy exists.

It has been shown that the application of a magnetic field causes a shrinking of the impurity atom wave functions, thereby reducing the interaction between neighboring impurity atoms.<sup>7</sup> In addition to causing a narrowing of the impurity band, the magnetic field can also cause the impurity band to split off from the conduction band, thereby producing a magnetically-induced energy gap.<sup>8, 9</sup>

This effect is illustrated schematically in Figure 2. The diagram in

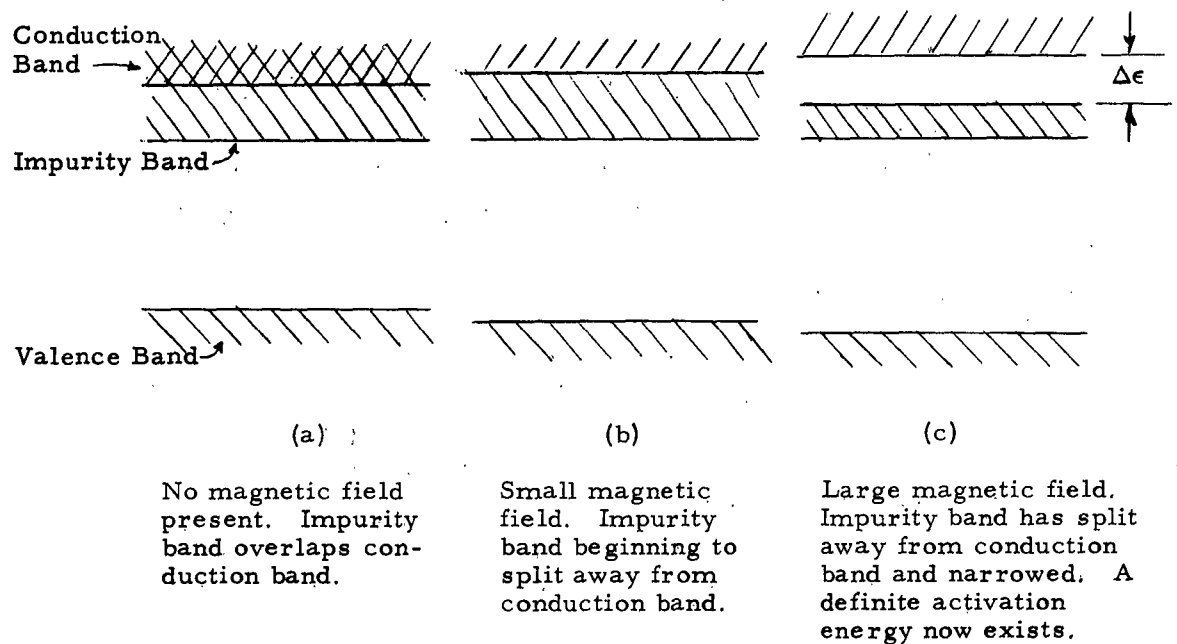


FIGURE 2

Figure 2(a) represents the situation where, in the absence of a magnetic field, the impurity band overlaps the conduction band. In Figure 2(b), the application of a moderate magnetic field causes the impurity band to begin to split away from the conduction band, and, in Figure 2(c), a larger magnetic field has produced a definite splitting with an energy gap,  $\Delta\epsilon$ .

As previously indicated, the magnetically-induced energy gap is brought about by a combination of two effects. The primary effect is a shift of the impurity energy levels with respect to the edge of the conduction band. As shown in Figure 2, the magnetic field causes the conduction band edge to move toward higher energies by an amount  $1/2 h\omega_c$  where  $\omega_c$  is the cyclotron frequency, defined by

$$\omega_c = \frac{eH}{m^*c} \quad (1)$$

with  $e$  the electronic charge,  $H$  the magnetic field strength,  $m^*$  the effective mass of an electron and  $c$  the speed of light. The impurity energy levels also shift to higher energies with application of a magnetic field;<sup>7</sup> however, they shift by a lesser degree than does the conduction band edge, thereby producing an increased separation between these levels and the edge of the conduction band (i. e. , an increased ionization energy).

The secondary effect of the magnetic field is to cause a narrowing of the impurity band. Since there is, at present, no theoretical analysis of this effect, its importance in the production of a magnetically-induced energy gap is unknown. However, since the width of the impurity band will depend critically on the concentration of impurity atoms in the indium antimonide, it may be possible to obtain experimental indications of the importance of this effect by studying samples with different impurity concentrations.

Recently, Putley<sup>10</sup> has made use of the magnetically-induced energy gap to construct a photoconductive detector for the submillimeter and millimeter wave region. This detector had a peak sensitivity at about 4.5 mm (comparable to the best thermal detectors), an extremely fast response time (less than a microsecond), and wavelength response extending at least to eight millimeters.

Putley<sup>11</sup> has made a rather cursory study of the phenomena by measuring the Hall effect and resistivity versus temperature, current versus electric field strength, photo-response versus current and photo-response versus wavelength,

all of these measurements also being performed at various magnetic field intensities up to about 800 gauss. His best detectors apparently come from very closely compensated material; however, no data on the effects of varying impurity densities have been reported.

An interesting feature of Putley's work which holds some possibilities for future developments is the observation of photoconductive response in InSb in the millimeter range, even in the absence of a magnetic field. This effect is attributed to absorption of the radiation by free carriers.<sup>11</sup> In absorbing energy from the radiation, the free carriers are excited to higher energy states in the conduction band. Now, at very low temperatures where the free carrier mobility is determined mainly by impurity scattering, a higher energy state in the conduction band corresponds to a state of higher mobility.<sup>12</sup> Thus, one observes an increase in conductivity on illumination of the material due to an increase in mobility (i. e. ,  $\Delta\sigma = ne\Delta\mu$ ) in contrast to the usual photoconductive effect where one observes an increase in conductivity on illumination due to an increase in the number of free charge carriers, the mobility remaining constant (i. e. ,  $\Delta\sigma = \Delta ne\mu$ ). Provided the time of relaxation from the high energy state back to the equilibrium energy state is not too short, the exploitation of this effect could possibly lead to a useful detector of millimeter waves which would not require a magnetic field.

## 2.0 THE DETECTOR MATERIAL

### 2.1 Hall Effect Analysis

Intensive studies by means of Hall effect and resistivity measurements were carried out on three samples of indium antimonide. The measurements were made in the liquid helium dewar, shown in Figure 3, using conventional dc techniques.<sup>13</sup> The samples were rectangular bars measuring approximately 1 x 2 x 8 millimeters which were prepared by lapping the surfaces in 600 mesh alundum powder and then cleaning in acetone. Broad area current contacts were made to the opposite 1 x 2 faces of the bars by coating with pure indium solder. By using clean indium and freshly prepared indium-antimonide samples, it was found that a good bond could be obtained without the use of a soldering flux. Small area electrical contacts for measurement of Hall and resistivity voltages were made along the 1 x 8 faces of the bars, as shown in Figure 4, and were also made with indium solder. The EMF's were measured with a high impedance voltmeter

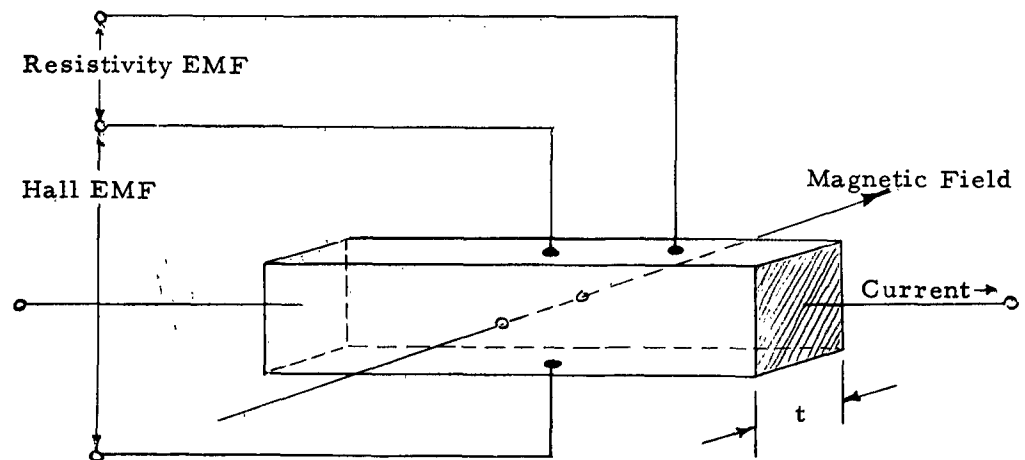


Figure 4: Configuration of Indium Antimonide Bars for Hall Effect and Resistivity Measurements.

(Hewlett - Packard Model 412A), and temperatures in the liquid helium range were measured with a carbon resistance thermometer.

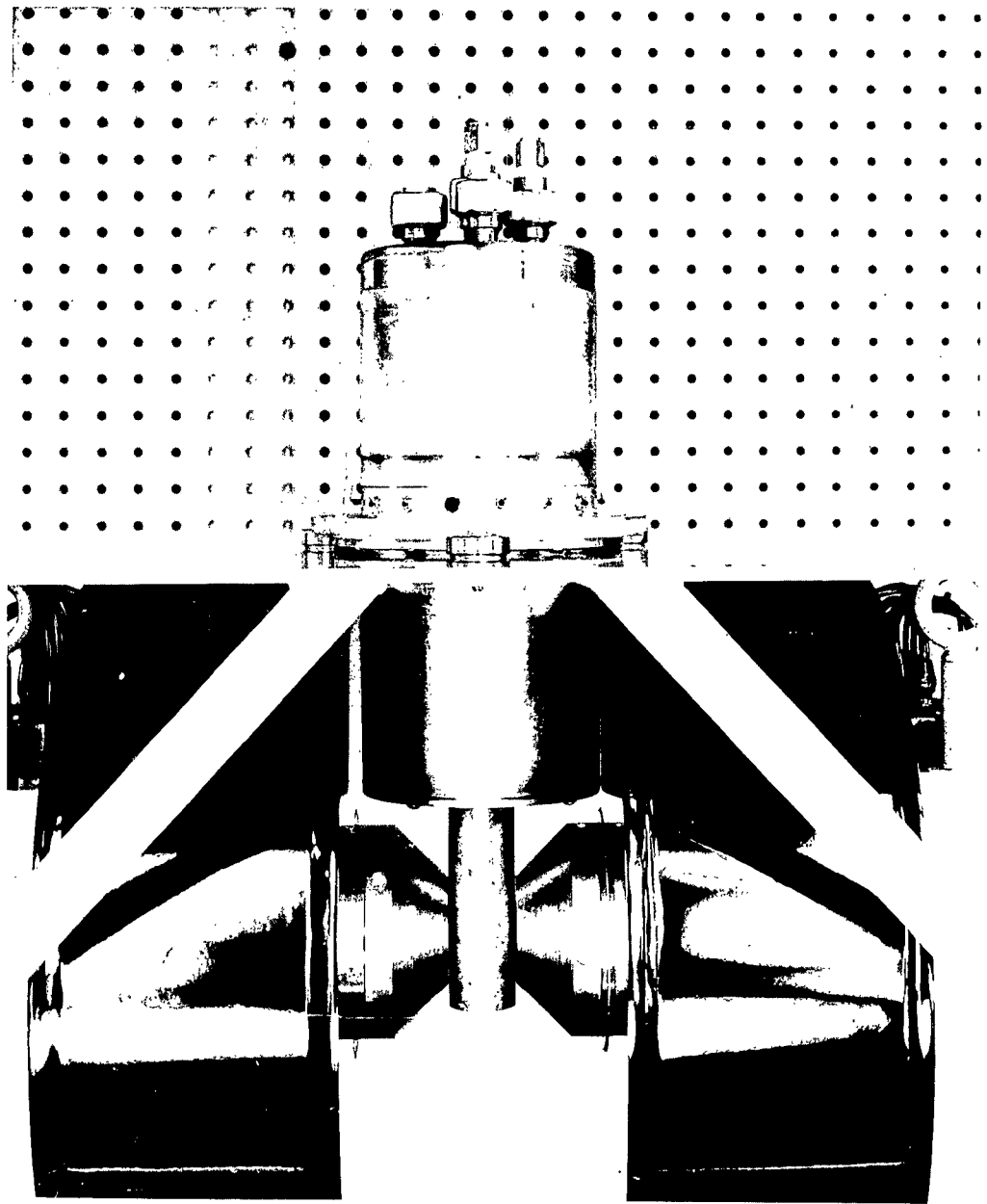


Figure 3. HALL EFFECT DEWAR MOUNTED IN ELECTROMAGNET

The Hall coefficient is defined by the equation,<sup>14</sup>

$$R_H = \frac{V_H}{I} \times \frac{t}{H} \times 10^8 \text{ (cm}^3\text{/coulomb)}, \quad (2)$$

where  $V_H$  is the measured Hall voltage,  $I$  is the current through the sample,  $t$  is the sample thickness, and  $H$  is the magnetic field strength. The factor  $10^8$  is a conversion factor for converting laboratory units (i. e., volts, amperes, gauss, centimeters) into the appropriate units for the Hall coefficient, indicated in Equation (2).

At room temperature, indium antimonide shows intrinsic behavior; therefore, Hall effect measurements at this temperature tell nothing about the concentrations of impurities in the material. At liquid nitrogen temperature (i. e., approximately 77°K), intrinsic charge carriers are unimportant and, therefore, the concentration of free charge is determined by the relative concentrations of donor and acceptor impurities. In this case, the net concentration of free charge carriers,  $n$ , is related to the Hall coefficient by

$$R_H = \frac{\gamma}{ne}, \quad (3)$$

with  $\gamma = \mu_H/\mu$ , and where  $e$  is the electronic charge (in coulombs);  $\gamma$  is the Hall coefficient factor, and  $\mu$  and  $\mu_H$  are, respectively, the conductivity mobility and the Hall mobility. The Hall coefficient factor,  $\gamma$ , is some number, close to unity, the precise value of which depends on the detailed scattering mechanisms which control the mobility and the energy distribution of the free charge carriers. Since this is not known in our case, we will simply assume that  $\gamma$  is unity in order to obtain an approximate analysis of the experimental data.

By combining measured values of Hall coefficient and resistivity, one obtains the Hall mobility,  $\mu_H$ , from

$$\mu_H = \frac{R_H}{\rho}, \quad (4)$$

where  $\rho$  is the resistivity.

Having determined the net free charge carrier concentration from the measured Hall coefficient using Equation (3), we then make the additional assumption that each donor (acceptor) atom contributes only one electron (hole) and, if all impurity atoms are ionized at liquid nitrogen temperature, then the net free charge concentration is

$$n = N_D - N_A \text{ (no. /cm}^3\text{)},$$

where  $N_D$  represents the concentration of donor atoms and  $N_A$  the concentration of acceptor atoms. Here we have assumed that  $N_D > N_A$  since this is the case of interest when dealing with n-type semiconductors.

Table I gives the essential characteristics of the three samples of indium antimonide which were determined from measurements at liquid nitrogen temperature.

TABLE I

Sample No.	Hall Coefficient $R_H$ (cm <sup>2</sup> /coulomb)	Net Impurity Concentration, $N_D - N_A$ (No/cm <sup>3</sup> )	Hall Mobility $\mu_H$ (cm <sup>2</sup> /volt sec)	Resistivity $\rho$ (ohm-cm)
IS-19	$7.4 \times 10^4$	$8.5 \times 10^{13}$	$2.2 \times 10^5$	.33
A	$2.0 \times 10^5$	$3.1 \times 10^{13}$	$3.2 \times 10^5$	.63
D	$3.6 \times 10^5$	$1.8 \times 10^{13}$	$1.0 \times 10^5$	3.7

Data obtained from Hall effect measurements in the liquid helium temperature range are shown for two of the three samples (Nos. A and D) in Figures 5 through 10. Consider, for the moment, the curves of Hall coefficient versus reciprocal temperature, Figures 5 and 8. These data can be interpreted in the following qualitative fashion. At low magnetic field intensity, the curves

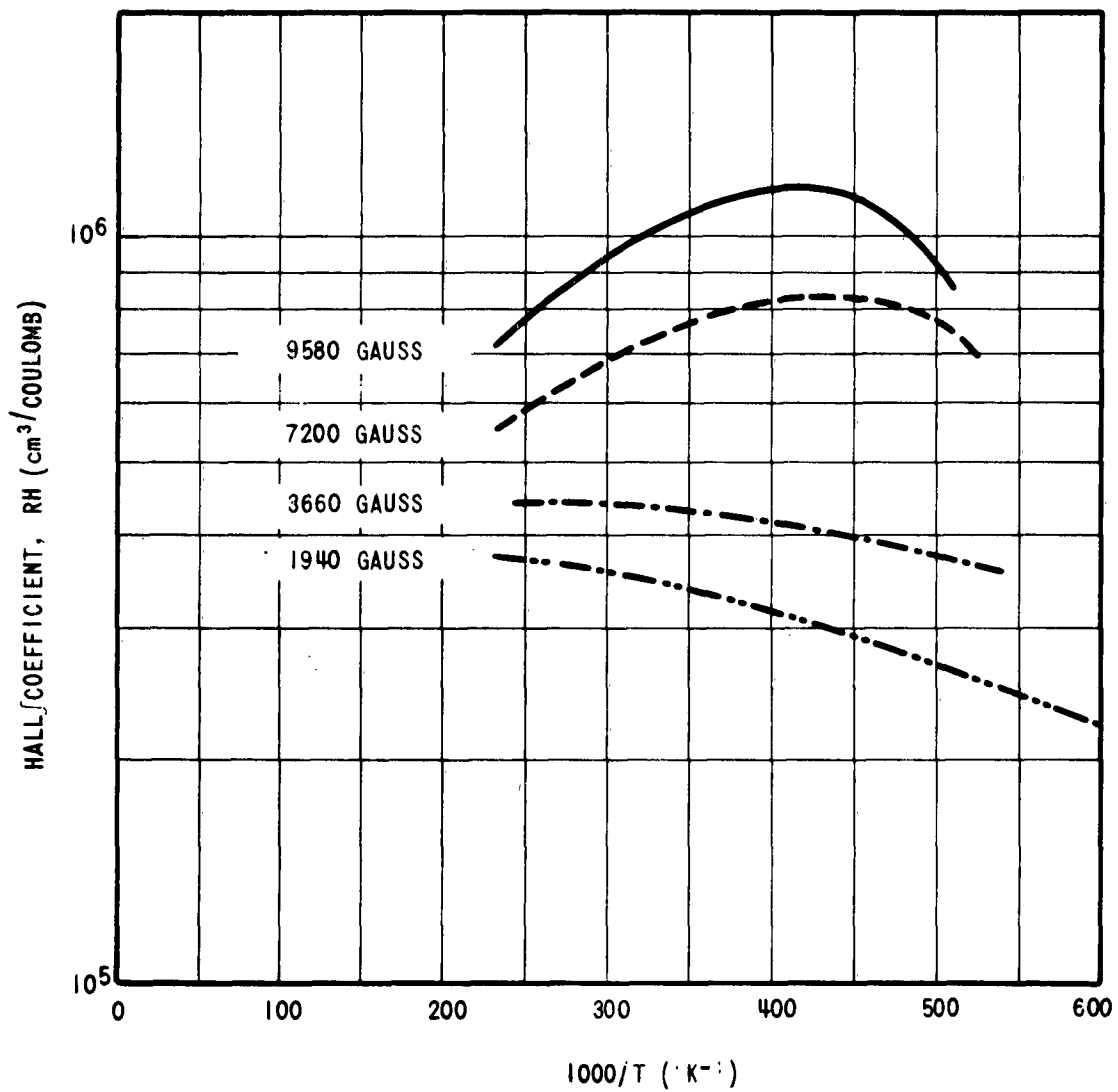


FIGURE 5 HALL COEFFICIENT vs. RECIPROCAL TEMPERATURE  
SAMPLE A

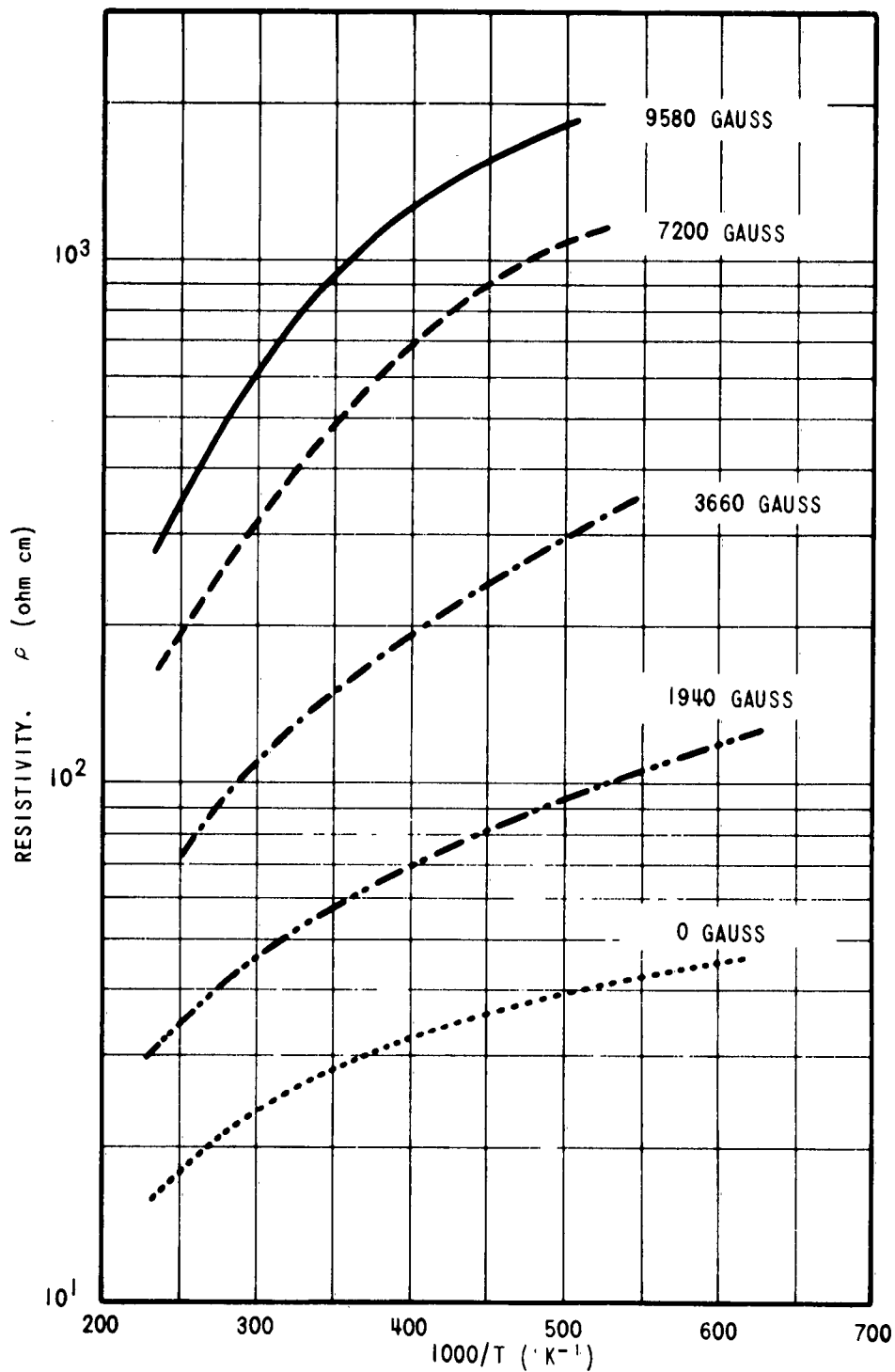


FIGURE 6

RESISTIVITY vs. RECIPROCAL TEMPERATURE  
SAMPLE A

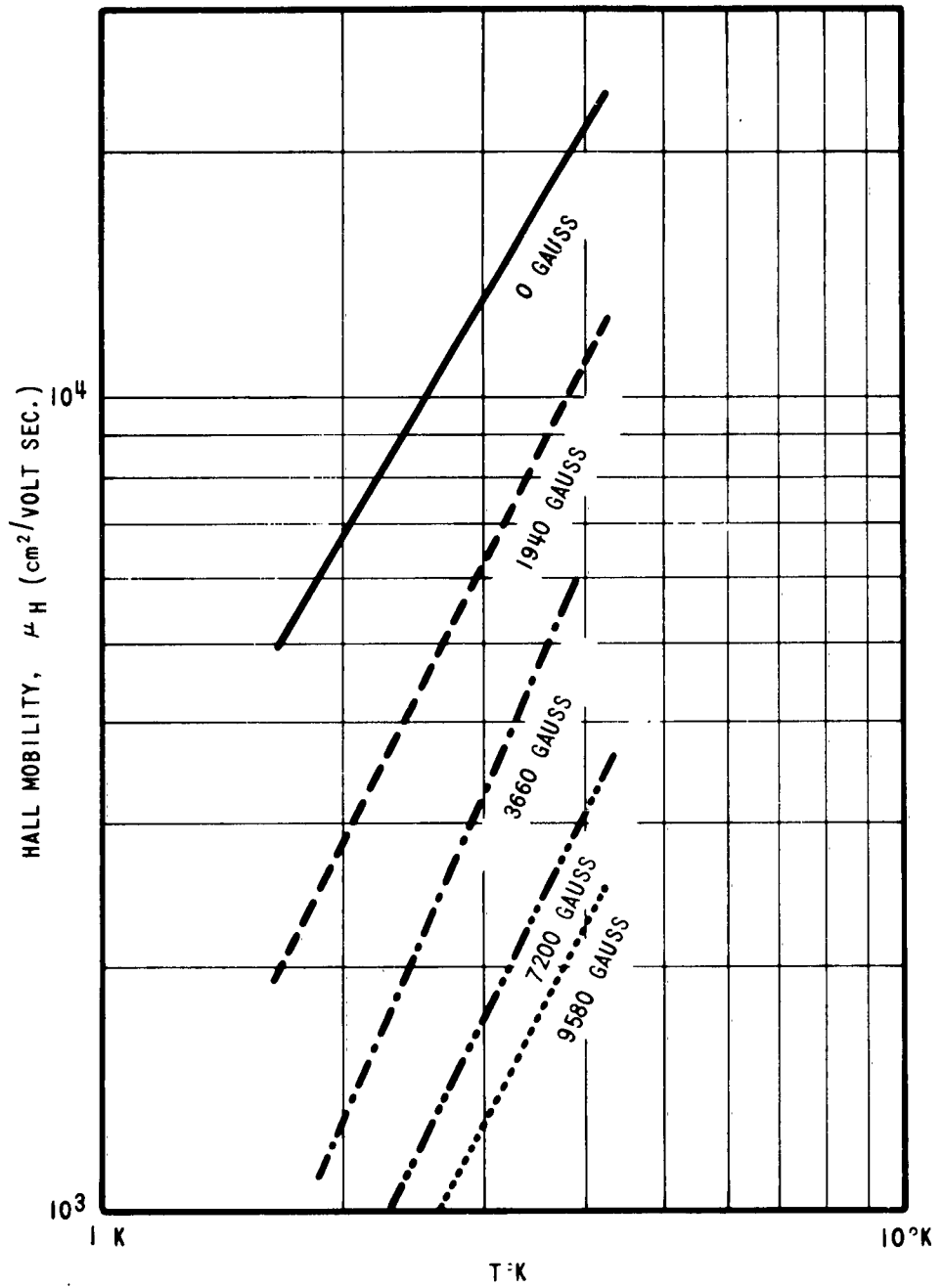


FIGURE 7

HALL MOBILITY vs. TEMPERATURE  
SAMPLE A

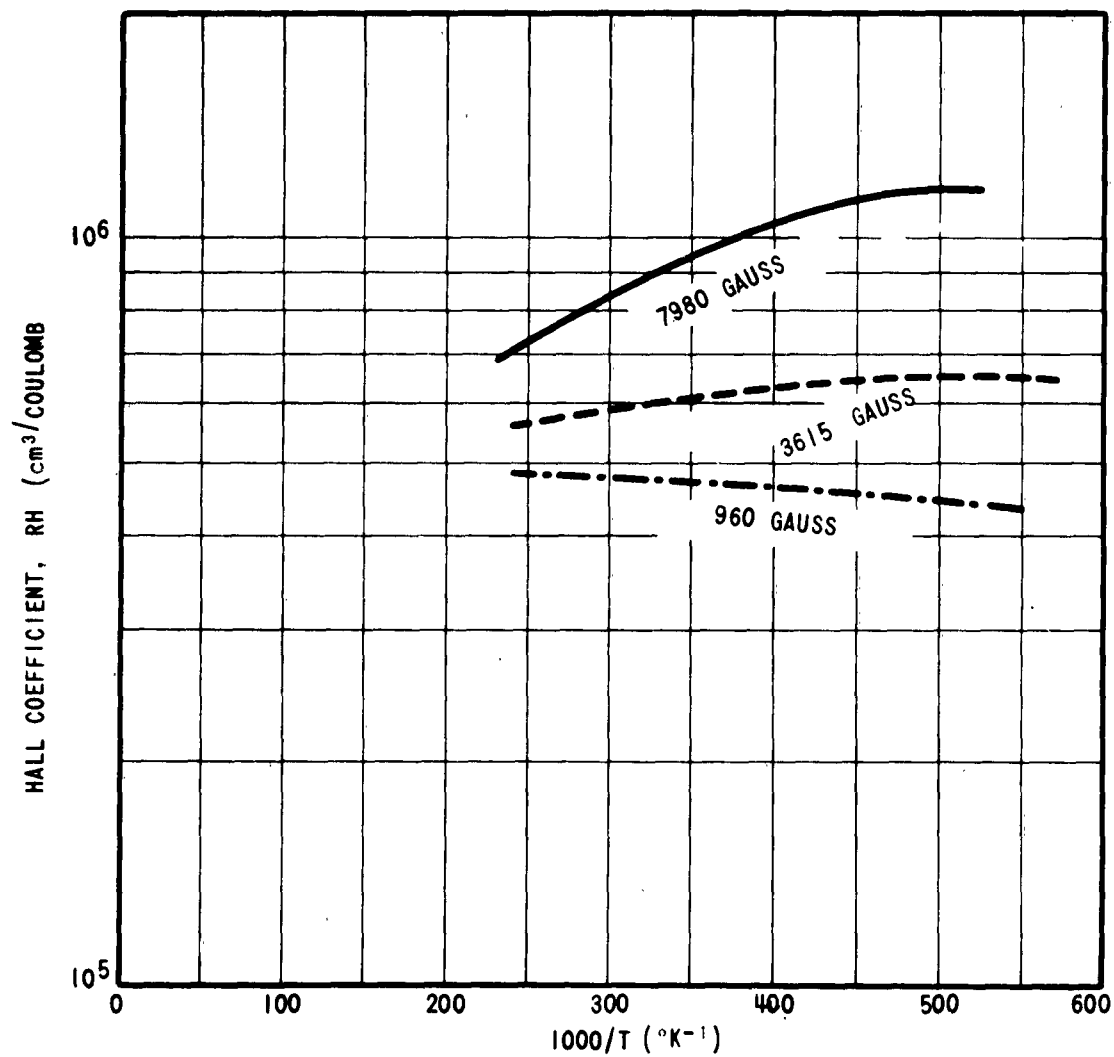


FIGURE 8 HALL COEFFICIENT vs. RECIPROCAL TEMPERATURE  
SAMPLE D

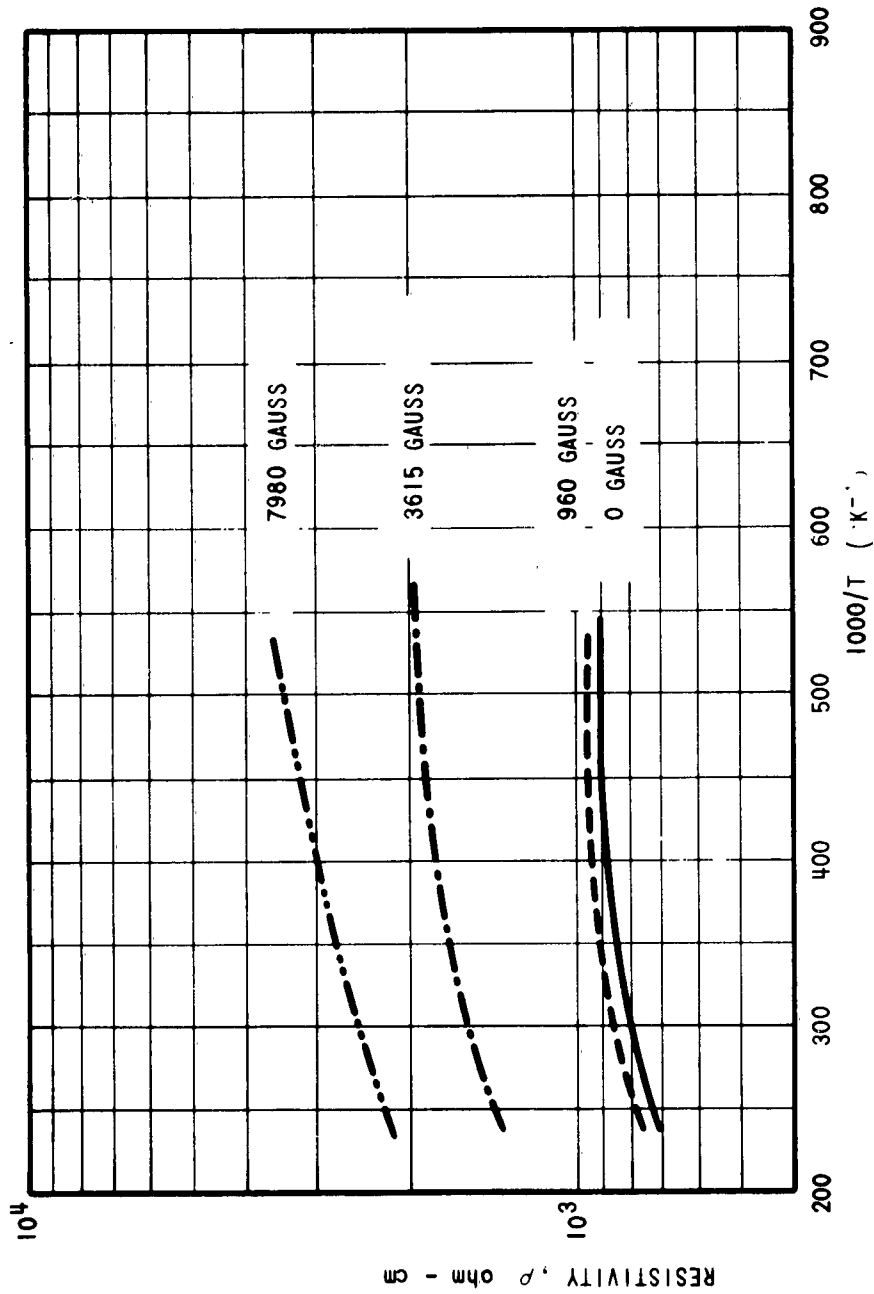


FIGURE 9 RESISTIVITY vs. RECIPROCAL TEMPERATURE

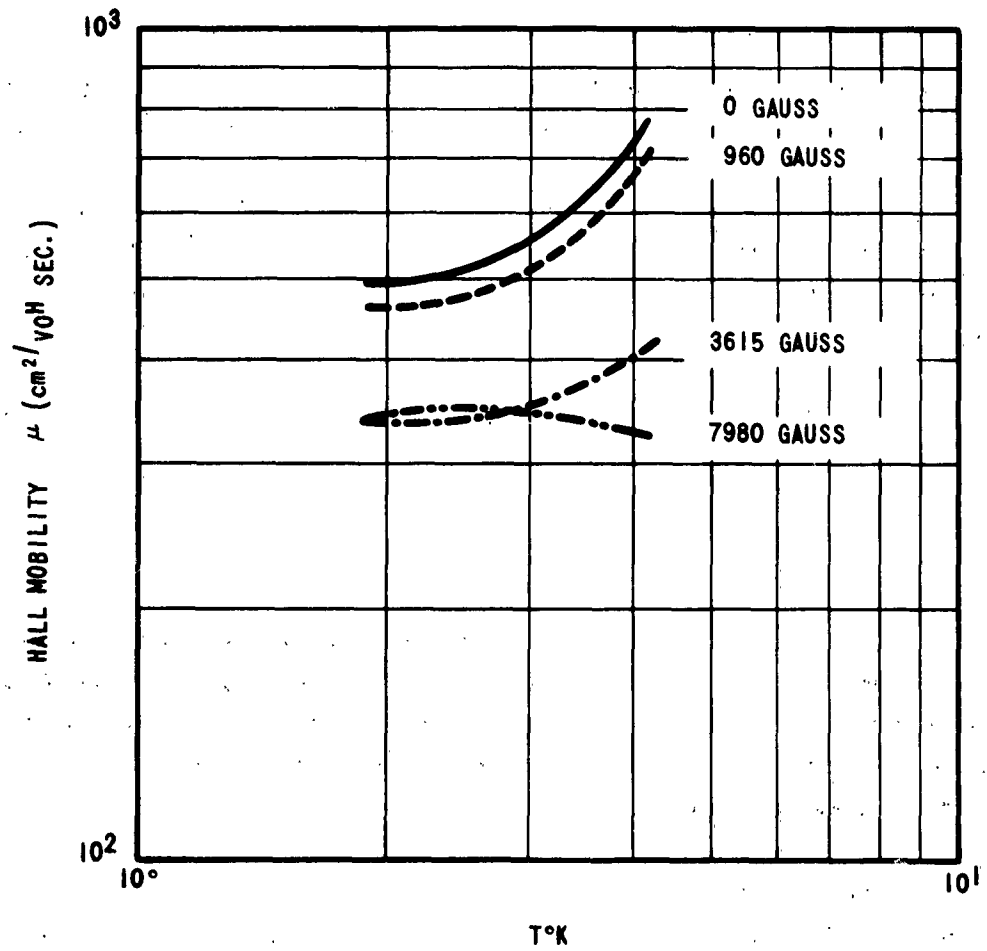


FIGURE 10 HALL MOBILITY vs. TEMPERATURE  
SAMPLE D

show little variation with temperature\* because no "freeze out" of free electrons onto the donor atoms takes place due to the fact that the impurity band overlaps the conduction band. As the magnetic field intensity is increased, the curves begin to take on a finite slope which is indicative of electron "freeze out" and the appearance of a magnetically induced energy gap.

A quantitative analysis of the data can be achieved by adopting a model of the conduction and impurity bands which involves the following assumptions.

a) With a sufficiently large magnetic field intensity, all of the conduction band electrons are constrained to the lowest Landau level. This condition will be satisfied, provided that the energy separation between Landau levels,  $h\omega_c$ , is much greater than the lattice energy,  $kT$ , that is

$$h\omega_c \gg kT \quad (5)$$

where

$$\omega_c = \frac{eH}{m^*c} \quad (6)$$

the quantity,  $\omega_c$ , is called the cyclotron resonance frequency,  $e$  is the electronic charge,  $H$  is the magnetic field intensity,  $m^*$  is the effective mass of a conduction electron and  $c$  is the velocity of light. By putting in numbers,\*\* it can readily be seen that this condition is easily satisfied at temperatures below  $4^\circ\text{K}$  for magnetic field intensities greater than about 1000 gauss.

b) The second assumption which we will make is that the separation between the Fermi level and the bottom of the conduction band is also much greater than  $kT$ . It will be seen later that this assumption is not so well justified as our first assumption; however, in order to keep the analysis tractable, we will utilize it.

---

\* The slight variation with temperature which does occur is probably due to the Hall coefficient factor,  $\gamma$ , which we are neglecting.

\*\* Electrostatic units are being used here and the electron's effective mass is taken as .013 times the free electron mass.

c) The third assumption we make is that conduction is significant only in one band, namely the conduction band; conduction in the impurity band is neglected.

Using these three assumptions, a statistical analysis of the distribution of electrons between bound states on donor atoms and free states in the conduction band yields the result,

$$\frac{(N_A + n) n}{N_D - N_A - n} = (2\pi m^* kT)^{1/2} \frac{eH}{h^2 c} \exp\left(\frac{-\Delta\epsilon}{kT}\right) \quad (6)$$

where  $n$  is the concentration of free electrons at some temperature,  $T$ , and the quantity  $\Delta\epsilon$  is the magnetically induced energy gap. The meaning of the other symbols is as previously described. For the case where  $n$  is much less than either  $N_A$  or  $(N_D - N_A)$ , Equation (6) can be written

$$n \approx \frac{(N_D - N_A)}{N_A} (2\pi m^* kT)^{1/2} \frac{eH}{h^2 c} \exp\left(\frac{-\Delta\epsilon}{kT}\right). \quad (7)$$

From this expression, we see that a plot of  $\log n$  versus  $1/T$  should have a straight line slope equal to  $(-\Delta\epsilon/k)$ . Since the Hall coefficient is inversely proportional to  $n$ , a plot of  $\log R_H$  versus  $1/T$  should have a slope of  $(+\Delta\epsilon/k)$ . Inspection of the experimental data show that a straight line slope does indeed appear, at least over part of the temperature range investigated. Furthermore, the slope increases with increasing magnetic field intensity, indicating an increasing energy gap.

In addition to yielding the magnitude of the magnetically-induced energy gap, the low temperature Hall data can also be used in conjunction with Equations (6) or (7) to obtain a value for the acceptor impurity concentration,  $N_A$ . Since the quantity  $(N_D - N_A)$  is already known from measurements at liquid nitrogen temperature, and the values of  $n$  and  $\Delta\epsilon$  at a given temperature and magnetic field intensity can be obtained from the data of Figures 5 and 8, the only unknown in these equations is  $N_A$  and thus we can solve for this quantity. For the case where  $n$  is not much less than  $N_A - N_D$ , better results are obtained by using Equation (6) rather than (7). On carrying out the calculations for the two samples, A and D, the results shown in Table II were obtained.

TABLE II

Sample No. A, $(N_D - N_A) = 3.1 \times 10^{13} \text{ cm}^{-3}$			
H (Gauss)	$\Delta\epsilon(\text{eV})$	$N_A (\text{cm}^{-3})$	$N_D (\text{cm}^{-3})$
9580	$3.9 \times 10^{-4}$	$11.0 \times 10^{14}$	$11.3 \times 10^{14}$
7200	$2.7 \times 10^{-4}$	$9.3 \times 10^{14}$	$9.6 \times 10^{14}$
Sample No. D, $(N_D - N_A) = 1.8 \times 10^{13} \text{ cm}^{-3}$			
H (Gauss)	$\Delta\epsilon(\text{eV})$	$N_A (\text{cm}^{-3})$	$N_D (\text{cm}^{-3})$
7980	$2.4 \times 10^{-4}$	$9.1 \times 10^{14}$	$9.3 \times 10^{14}$

Perhaps the most interesting result obtained from this analysis is that the actual donor and acceptor atom concentrations in the crystal are about  $10^{15}$  per  $\text{cm}^3$  and, because of the very close balance between the two concentrations, the net impurity concentration,  $(N_D - N_A)$ , is very much smaller, being about  $2$  to  $3 \times 10^{13}$  per  $\text{cm}^3$  for the two samples. Thus, we conclude that these samples are not nearly as pure as one might be led to think from the liquid nitrogen temperature Hall data alone (i. e., Table I). Further support for this conclusion is obtained from the mobility values at liquid nitrogen temperature. These are seen to be  $3.2$  and  $1.0 \times 10^5$   $\text{cm}^2/\text{volt sec}$ . For very pure indium antimonide, the electron mobility at this temperature should be greater than  $5 \times 10^5$   $\text{cm}^2/\text{volt sec}$ , thus the lower mobility values for our samples are compatible with a relatively high impurity content.

Further interesting properties of these samples may be deduced from the liquid helium temperature mobility measurements; however, before going into this, we want to point out that the values of  $N_D$  and  $N_A$  obtained from analysis of the one-band conduction model must be considered only as rough approximations because of the assumptions which were necessarily made. In particular, assumptions (b) and (c) may not be very well justified for the samples used here. With regard to assumption (b), when the magnetically-induced energy gap is produced, the Fermi level can be considered to lie about half-way between the impurity band and the bottom of the conduction band. Therefore, the position of the Fermi level,  $\epsilon_c - \epsilon_F$ , will always be less than the energy gap,  $\Delta\epsilon$ . This is illustrated in Figure 11. Since we have found values for the energy gap of the order of  $3$  to  $4 \times 10^{-4}$  eV., the condition that  $\epsilon_c - \epsilon_F \gg kT$  is not satisfied at  $4^\circ\text{K}$  and becomes satisfied only for temperatures of the order of  $1^\circ\text{K}$  or lower. However, at these

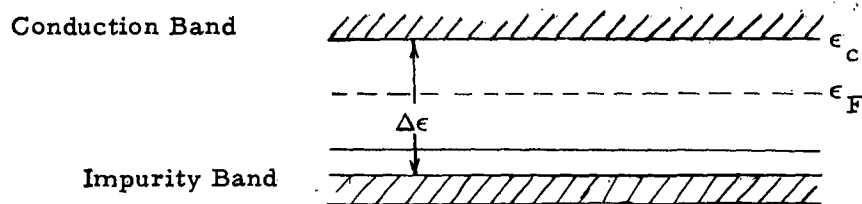


Figure 11. Approximate position of Fermi energy,  $\epsilon_F$ , with respect to conduction band edge,  $\epsilon_c$ , and impurity band.

temperatures, impurity band conduction becomes important, and assumption (c) can no longer be satisfied. Impurity band conduction manifests itself by causing the curve of Hall coefficient versus  $1/T$  to break from a positive slope over into a negative slope as the temperature is lowered. This may be seen in Figures 5 and 8 at temperatures below about  $3^{\circ}\text{K}$ .

Thus, it appears that a more accurate analysis for our samples must be based on a two-band model which uses Fermi statistics in place of Maxwell-Boltzmann statistics and also includes conduction in the impurity band. Such an analysis, although much more difficult than our simple approximation, can be carried out, as has been shown by Sladek.<sup>9</sup> It would be interesting to carry this out for our samples but this must await future work. For the present, we must accept the results of the simple analysis, recognizing, of course, that they are just approximate values.

Consider now the mobility measurements at liquid helium temperatures shown in Figures 7 and 10. We see that sample D shows very much smaller mobility values than does sample A, as well as having a different temperature dependence. Since the Hall coefficient data indicated that both samples had about the same total impurity content, the lower mobility for D cannot be attributed to additional impurity scattering. We must conclude then, that D has some other type of scattering centers which cause the reduced mobility. This could be provided by defects in the crystal lattice such as dislocations.

The temperature dependence of mobility found for A is similar to some of the n-type indium antimonide samples measured by Putley<sup>15</sup> which were successfully interpreted in terms of ionized impurity scattering.

## 2.2 Photoconductive Response

The photoconductive response of three different samples has been measured. The first sample (A) was a Hall sample 8 mm x 2 mm x 1 mm thick; whereas the other two samples (B and C) were both squares 5 mm x 5 mm x 3 mm thick. After cutting the detector samples, (B) was rinsed with ionized water

before mounting, while the sample (C1) was first etched in a mixture of hydrochloric and nitric acid and was then washed with demineralized deionized water before being mounted. Later on, in the course of the experiments, the detector sample (C1) was reprocessed by lapping, and the sides were sandblasted to remove the effect of the etching; the sample was then identified as C2.

The rf radiation sources were two klystrons; an EMI R5146 tube operating at 8 mm wavelength (35 Gc) and a Raytheon QK369 tube operating at 4 mm (70 Gc). To obtain radiation at the 2 mm wavelengths, an F. X. R. crystal harmonic generator was used which had a conversion loss of 25 to 30 db. A standard gain horn was employed to irradiate the detector samples. The EMI tube had a nominal power of 50 milliwatts at 35 Gc, and the Raytheon tube gave 14 milliwatts at 70 kMc. This equipment is shown in Figure 12.

For photoconductivity measurements, the sample is connected in series with a battery and load resistor as shown in Figure 13. The output from the detector load resistance was fed into a Tectronics Type 122 low-level preamplifier and then into a General Radio type 1554-A sound analyzer. A series of different load resistances were tried, and finally an optimum load of 0.1 Meg Ohm was chosen. Instead of using a mechanical chopper, the klystron output was modulated with a 1000 cycle/sec square-wave generator. The detectivity  $D^* = (S/N)\Delta f^{1/2}/PA^{1/2}$  was calculated for the samples at different wavelengths of 2 mm, 4 mm and 8 mm. In the above expression for  $D^*$ ,  $S/N$  is the signal-to-noise ratio of the amplifier,  $\Delta f$  is the bandwidth of the amplifier,  $P$  is the power density of radiation and  $A$  is the effective area of the detector. In all the measurements which were performed, the noise figure was determined by the amplifier noise, and this figure remained constant as the magnetic field or the bias was changed. The average figure for the noise was about 0.17 volts for  $\Delta f \approx 72$  cps. The sample was cooled as is illustrated in the drawing of Figure 14 to the temperature of liquid helium by thermal conduction thru the copper mount to the liquid helium reservoir. Pumping over the liquid helium chamber of the dewar to reduce the temperature of the sample below 4.2°K when the sample was irradiated with 4 mm radiation did not increase the detectivity appreciably. Since the detectivity for samples B and C2

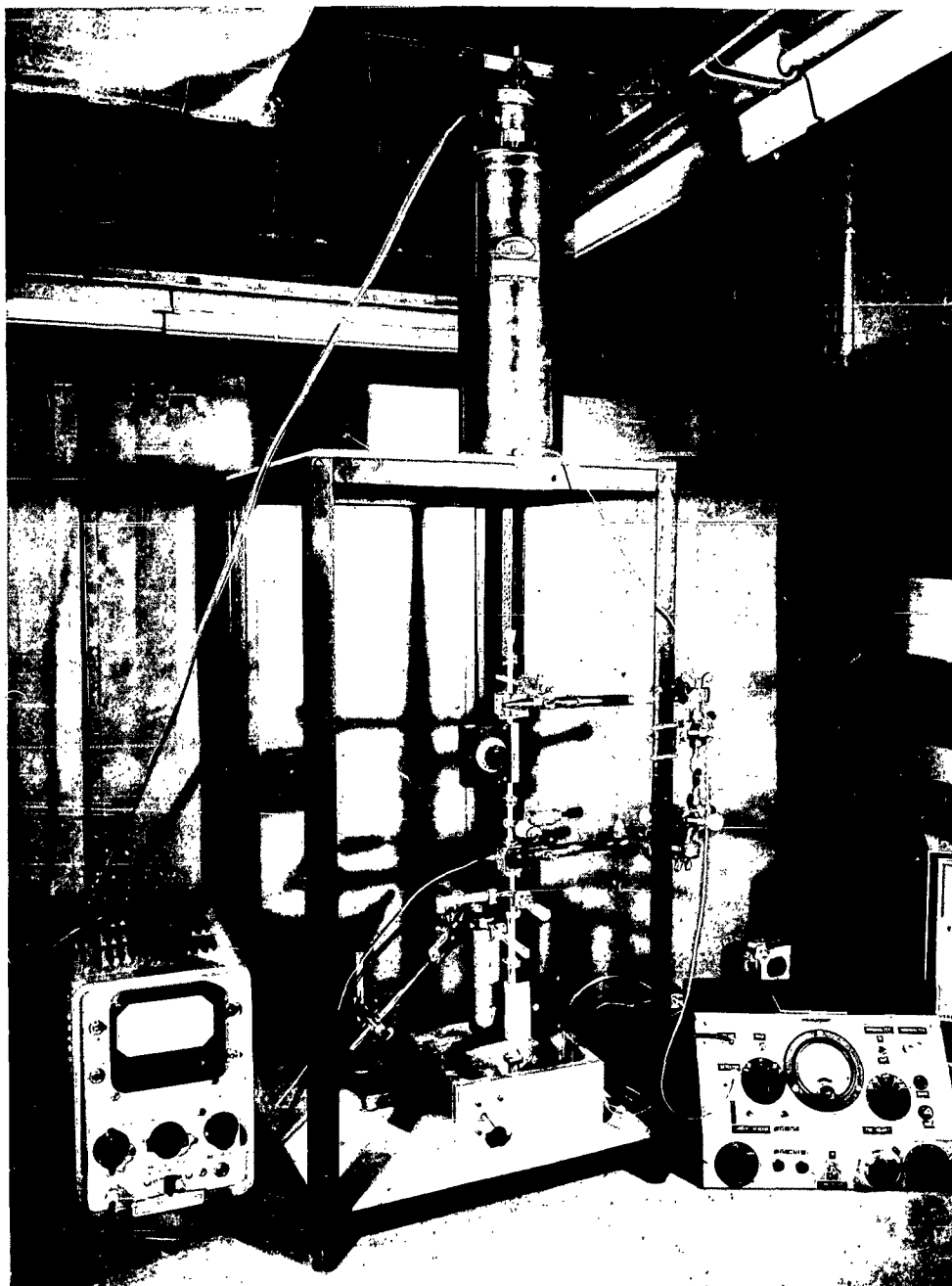


Figure 12. MILLIMETER WAVE GENERATING EQUIPMENT,  
DETECTOR, AND ASSOCIATED ELECTRONIC EQUIPMENT

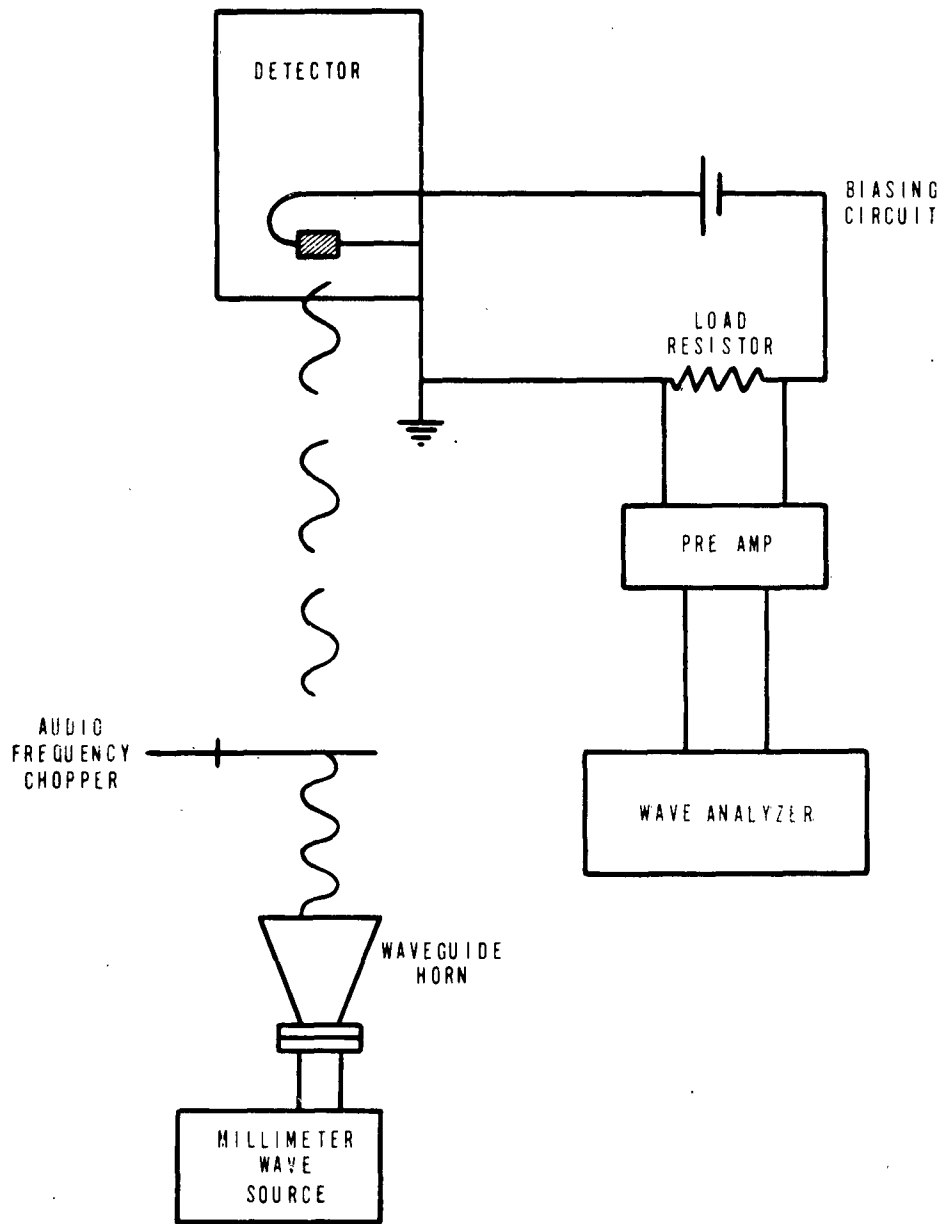
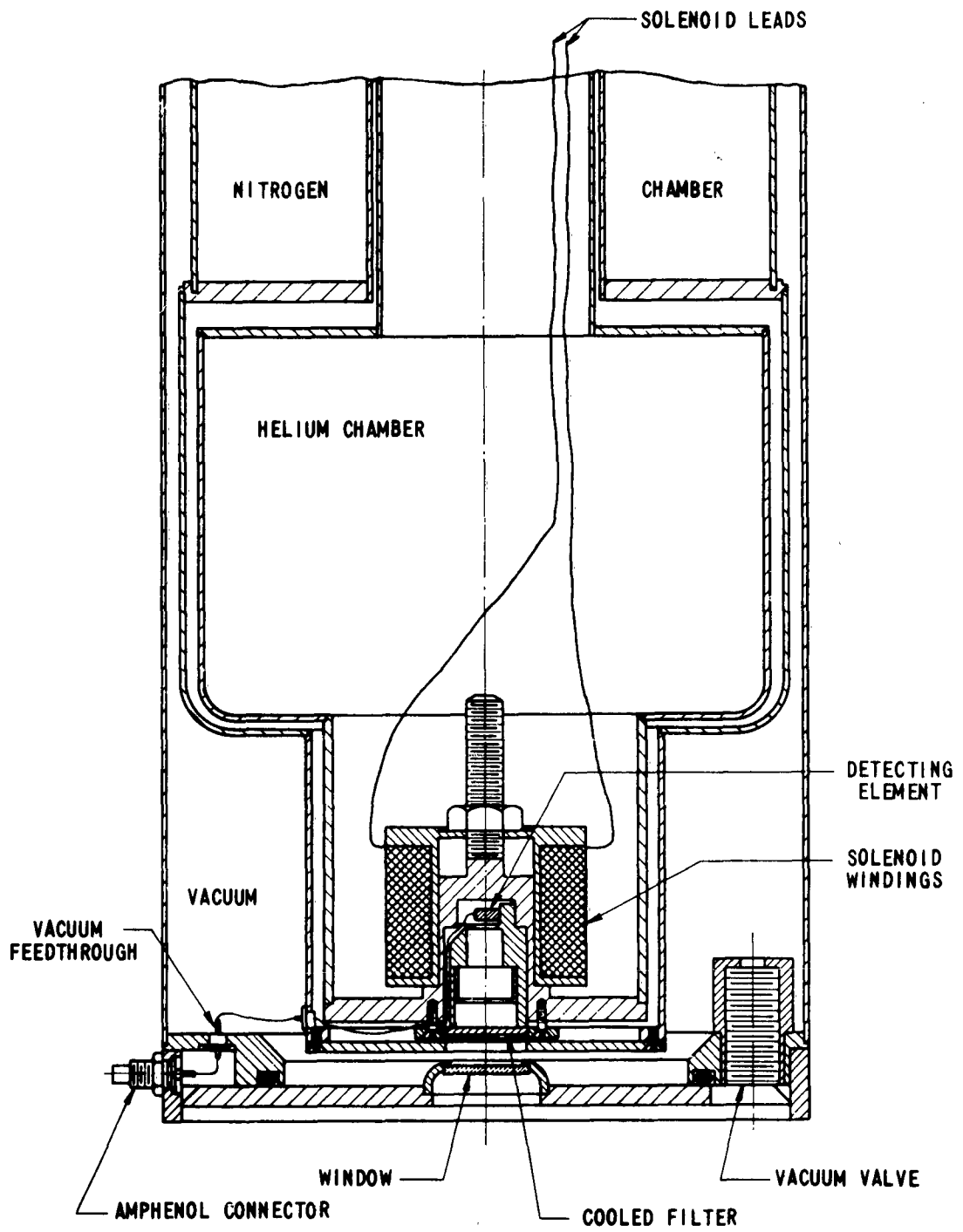


FIGURE 13

BIASING CIRCUIT SCHEMATIC AND OTHER ASSOCIATED TEST EQUIPMENT FOR MILLI-METER WAVE DETECTOR.



MILLIMETER WAVE DETECTOR PACKAGE WITH IMMERSSED SOLENOID

FIG. 14

were quite high (in the order  $10^{10}$  at 4 mm) we have concluded that for this particular sample at these wavelengths it is not really necessary to operate the detector with a vacuum pump and that a temperature of 4.2°K may be adequate for most purposes. However, sample A, which was tested in another dewar for Hall effect at temperatures from 2.6 degrees K to 4.66°K showed the signal voltage three times as large at the lower temperatures.

A curve showing the change in resistance of the samples B and C2 with the magnetic field is shown in Figure 15. Sample C2 shows a rate of 3.356 ohm increase per gauss while B has a 0.2 ohm increase per gauss. Despite such an increase in the resistance, both samples displayed the same detectivity at 4 millimeters. All the detectivity curves which are shown in Figures 16 through 20 were measured on samples which were mounted within the superconducting solenoid. Figure 16 shows the signal-to-noise ratio of the B detector sample at 8 mm as a function of the bias current for seven different magnetic field settings. It is noticed that at low bias currents the magnetic field helps to increase the S/N ratio while, at higher bias currents, the S/N ratio is greater without field. In general, the application of the magnetic field at the optimum bias decreased the detectivity by about 20 percent. The detectivity  $D^*$  (8 mm, 1000, 1), as measured from the data shown in Figure 16 for the best signal-to-noise ratio, was about  $1.05 \times 10^{10}$  cm cps<sup>1/2</sup>/watt. Figures 17 to 19 show the signal-to-noise ratio as a function of bias current for samples B, C1 and C2 at 4 mm and at different magnetic fields. We again see that the sensitivity is greatest at zero magnetic field for all the samples. For the etched sample C1 shown in Figure 18 the signal-to-noise ratio is an order of magnitude lower than sample B. The sample C1 was then taken out, lapped and sandblasted at the sides and then mounted as sample C2. The result of signal-to-noise ratio versus bias current is shown in Figure 19. We see that without magnetic field the sensitivity remains constant with changes in the bias current but as soon as the magnetic field is applied the detectivity decreases rapidly with both an increase in the magnetic field and the bias current. The detectivity  $D^*$  (4 mm, 1000, 1) at 4 mm for the non-etched sample was about  $10^{10}$  cm cps<sup>1/2</sup>/watt.

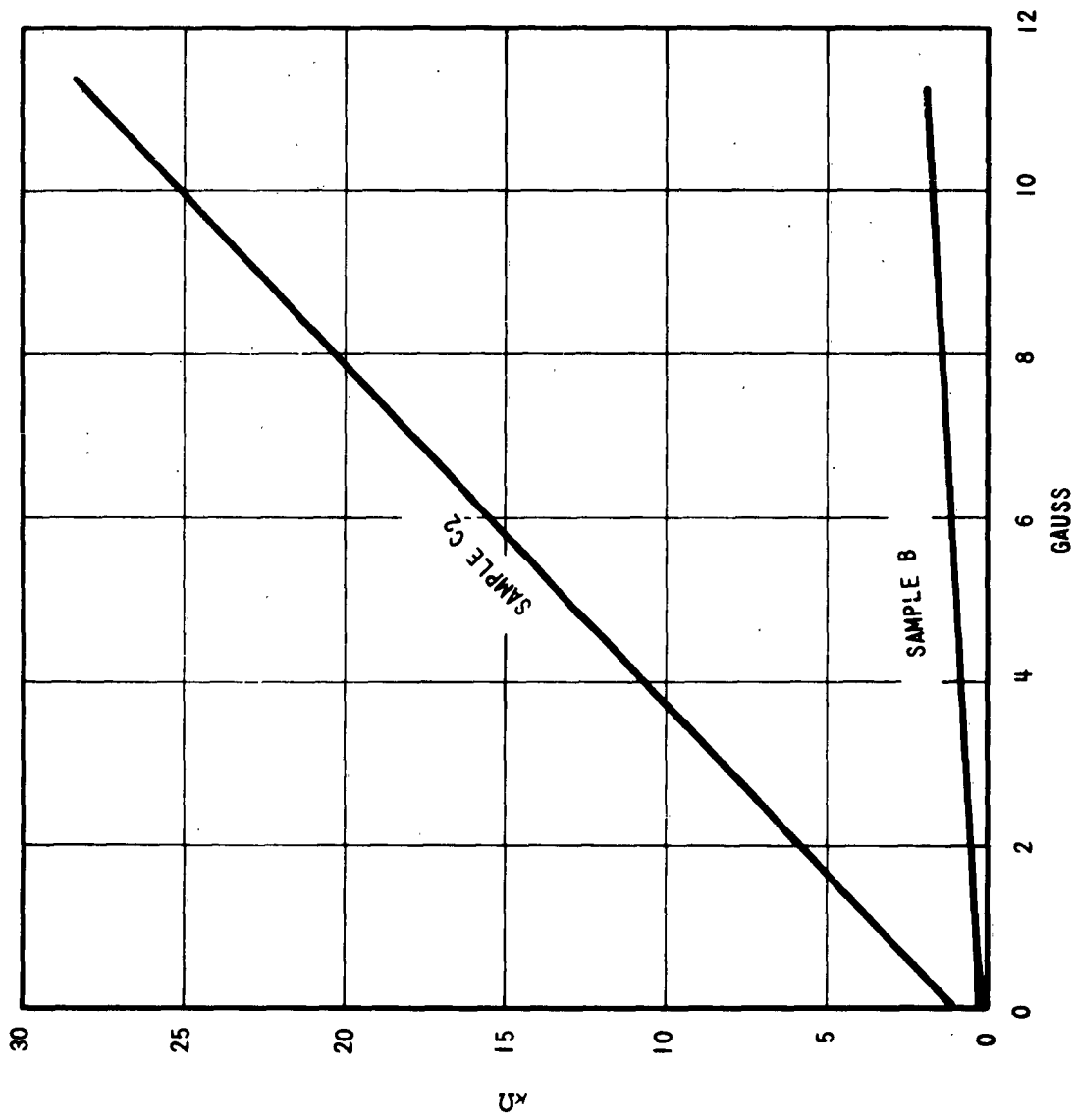


FIGURE 15 THE D.C. RESISTANCE OF SAMPLES B AND C<sub>2</sub> AS A FUNCTION OF THE MAGNETIC FIELD

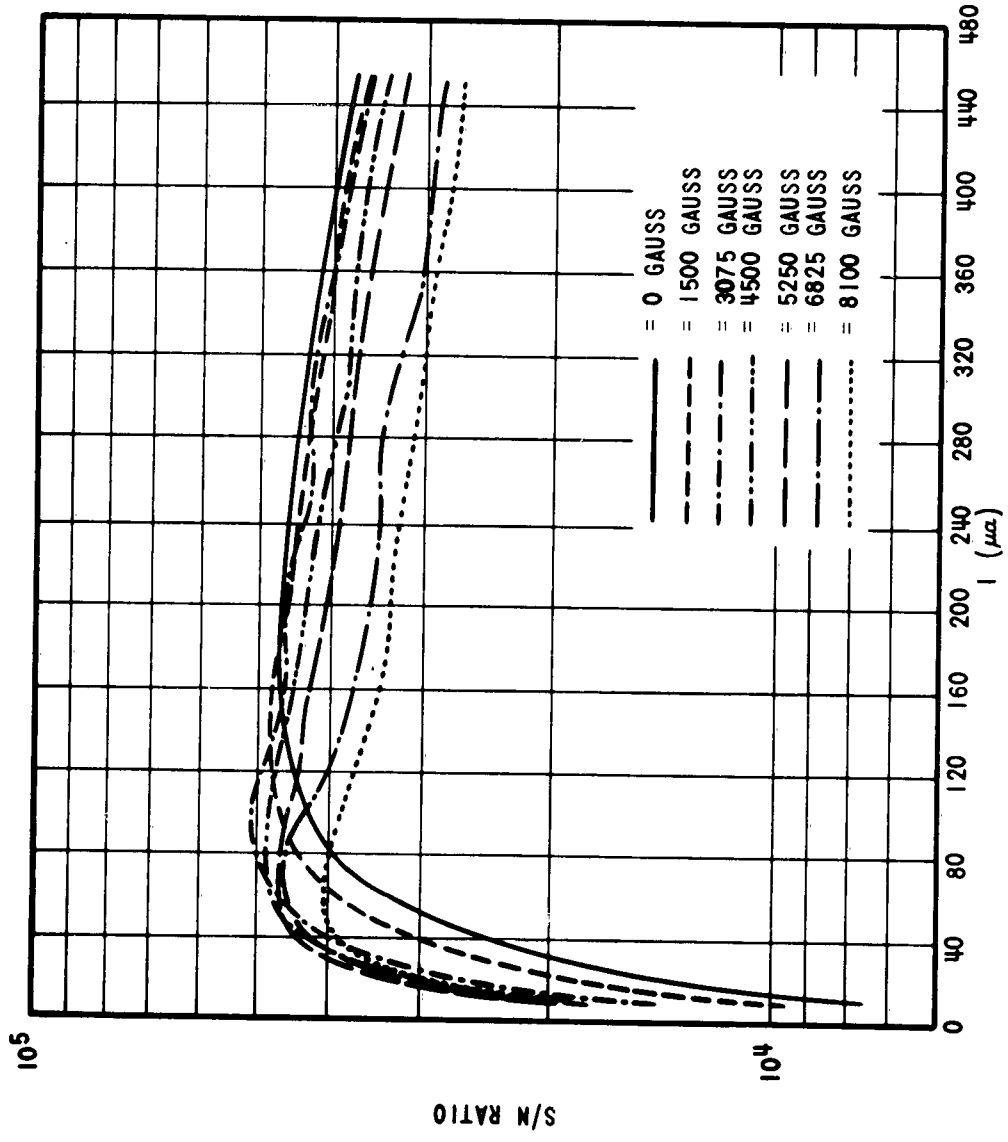


FIGURE 16 SIGNAL TO NOISE RATIO OF In-Sb SAMPLE B AS A FUNCTION OF THE BIAS CURRENT AT 8mm INPUT SIGNAL.

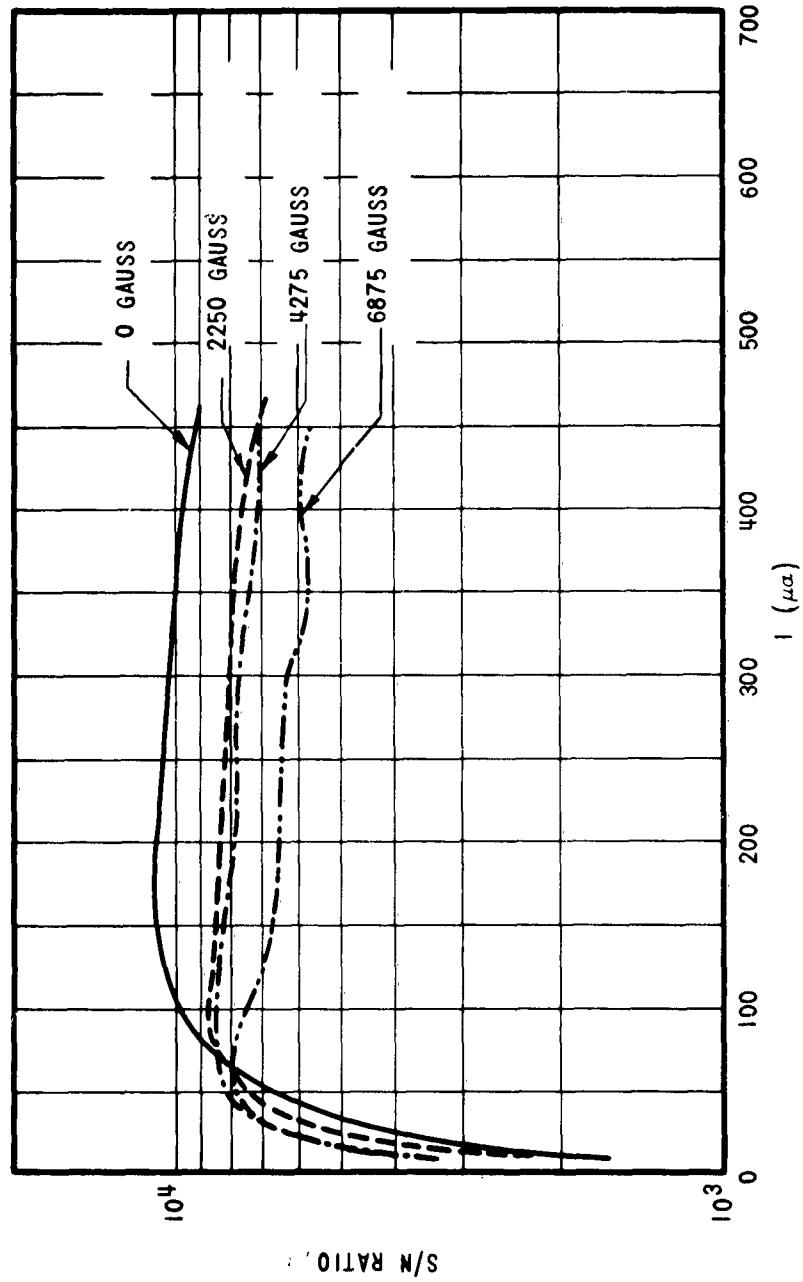


FIGURE 17 SIGNAL TO NOISE RATIO OF In-Sb SAMPLE B AS A FUNCTION OF THE BIAS CURRENT AT 4mm INPUT

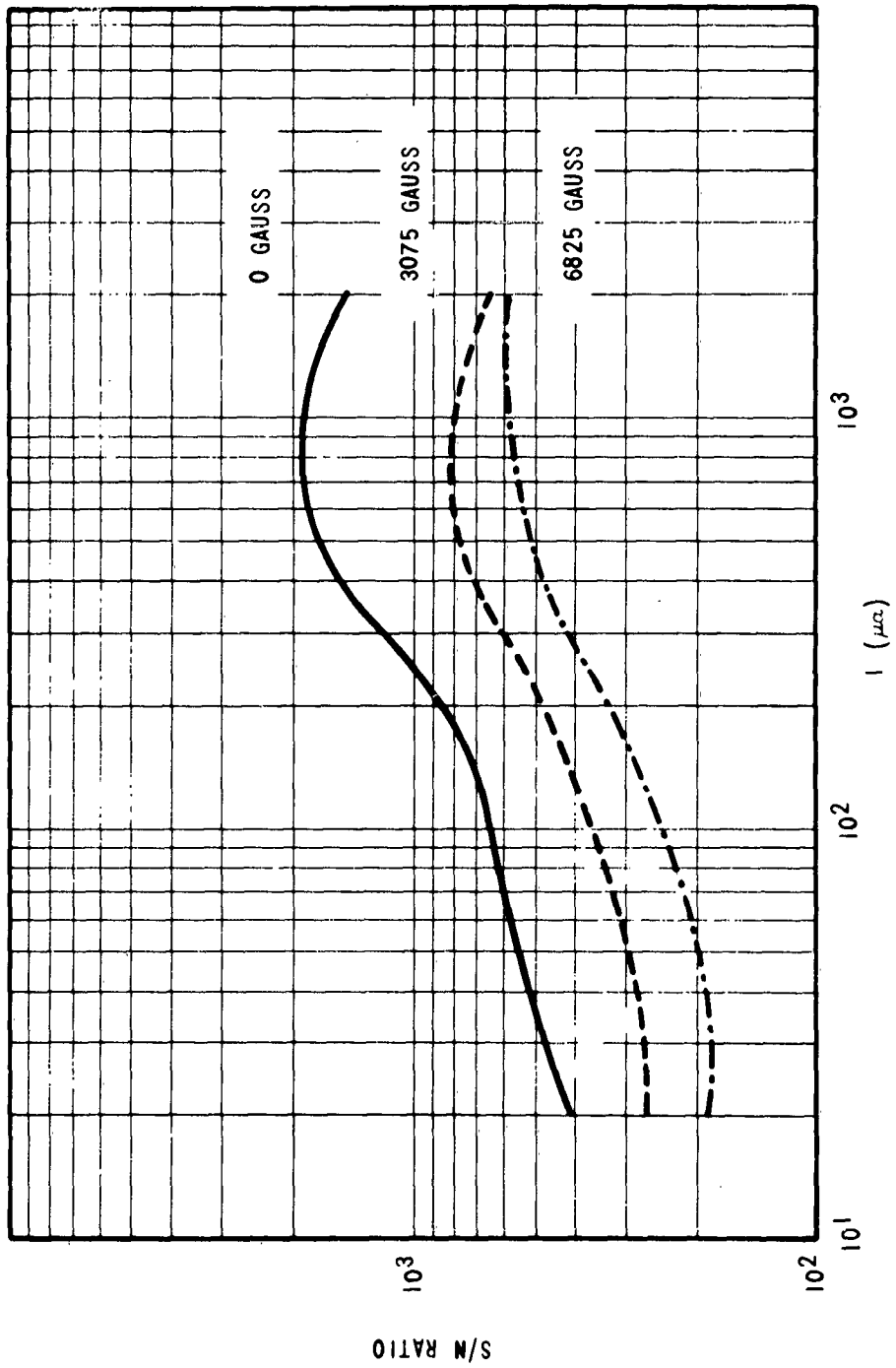


FIGURE 18  
 SIGNAL TO NOISE RATIO OF THE  $\text{InSb}$  SAMPLE C1  
 AS A FUNCTION OF CURRENT AT 4mm INPUT BIAS

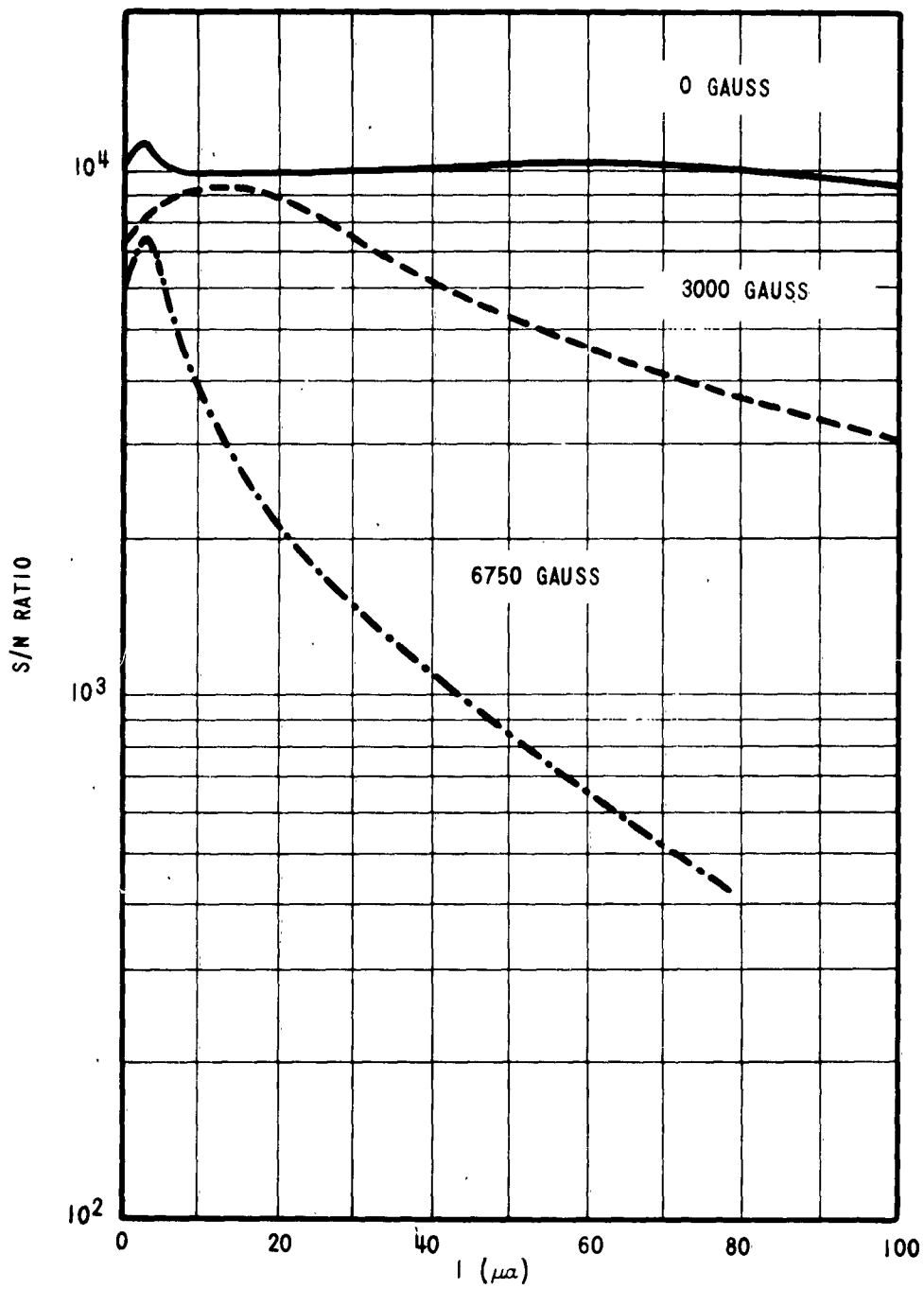


FIGURE 19 SIGNAL TO NOISE RATIO OF THE InSb SAMPLE C<sub>2</sub> AS A FUNCTION OF BIAS CURRENT AT 4mm INPUT

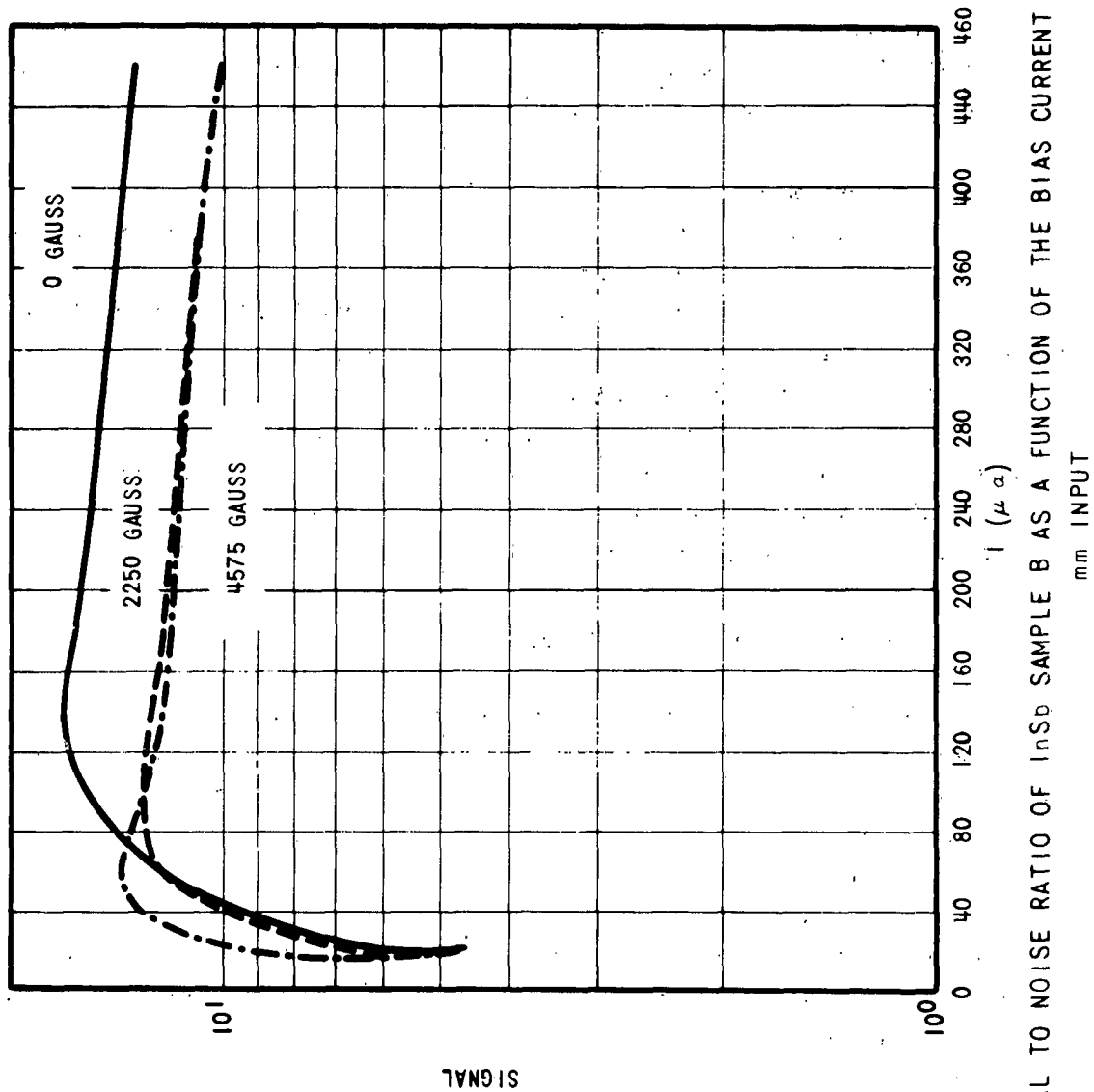


FIGURE 20 SIGNAL TO NOISE RATIO OF InSb SAMPLE B AS A FUNCTION OF THE BIAS CURRENT AT 2

mm INPUT

SIGNAL

Almost the very same effects are observed at the 2 mm wavelength. The application of the magnetic field reduces the signal at higher bias currents. The few samples which were tried, all have shown a definite decrease in signal-to-noise ratio with the application of the magnetic field except when relatively high bias currents have been used, Figure 20. The detectivity at 2 mm, taking the best possible conversion ratio for the harmonic generator and assuming no losses in the horn, has been  $1.1 \times 10^{11}$  cm cps<sup>1/2</sup>/watt.

It is interesting to note that, at the higher bias currents used, the detectivity of these samples for radiation in the 2 to 8 mm range decreases when the magnetic field is applied. This is in contrast with the behavior reported by Putley where the detectivity increases with application of the magnetic field. However, we hasten to point out that Putley's observations were made for radiation in the 0.1 to 1.5 mm range, while ours is for radiation in the 2 to 8 mm range. It is not expected that our samples will show any different behavior than Putley's when being used to detect submillimeter wave radiation. These results do emphasize, however, that the photoeffects being observed are quite complex and will require some further study.

### 2.3 The Absorption Coefficient

In order to evaluate roughly the absorption coefficient of the n-type InSb at different wavelengths, a 4 mm thick slab of the material was placed inside the dewar in front of the detector crystal. This piece was mounted inside the superconducting solenoid and was cooled to the same temperature as the detector and was thus subjected to the same conditions of the detector crystal. The detector was then subjected to electromagnetic radiation from a klystron. The attenuation due to the presence of the InSb was measured at different magnetic fields. The attenuation remained constant with the field as both the detector crystal and the attenuator piece were seeing the same magnetic field. One can write for the attenuation factor,

$$\frac{I}{I_0} = (1-R) \exp(-\alpha x),$$

where  $x$  is the thickness of the attenuator piece,  $\alpha$  is the attenuation constant,

R is the reflectivity, and  $\frac{I}{I_0}$  is the attenuation factor, or in other words is the ratio of the intensity of the electromagnetic radiation at the entrance face to that at the exit face of the attenuator.

Solving for  $\alpha$ , we have

$$\alpha = \frac{1}{x} \log_e \frac{I_0}{I} (1-R). \quad (\text{cm}^{-1})$$

In the determination of the coefficient of reflection, there is an impedance matching problem and one has to calculate the reflectivity R for every wavelength separately. At microwave frequencies, the thickness of the attenuating piece is of the same order of magnitude as the wavelength, and if, for example, the attenuating piece is a quarter of a wavelength thick, no energy would be reflected.

For a piece of material  $l$  cm thick, the coefficient of reflection is

$$\rho = \frac{\eta_0 - Z_L}{\eta_0 + Z_L},$$

where  $\eta_0 = \sqrt{\frac{\mu_0}{\epsilon_0}}$  is the impedance for the free space. Here,  $\mu_0$  is the permeability and  $\epsilon_0$  is the dielectric constant.  $Z_L$  is the impedance of the attenuating piece and is equal to

$$Z_L = \eta_2 \frac{n \cos kl + i \sin kl}{\cos kl + i n \sin kl},$$

where  $\eta_2 = \sqrt{\frac{\mu_2}{\epsilon_2}}$ ;  $\mu_2$  is the permeability of the attenuator,  $\epsilon_2$  is its dielectric constant,  $n$  is the coefficient of refraction, and  $k$  is the propagation constant in the attenuator.

$$k = \frac{2\pi}{\lambda_{\text{atten.}}} = \frac{2\pi n}{\lambda_{\text{free space}}}$$

and

$$\eta_2 = \sqrt{\frac{\mu_2}{\epsilon_2}} \approx n \eta_0$$

$$n = \sqrt{\frac{\epsilon_2}{\epsilon_0}}$$

At 8 mm we have found  $\rho = 0$  for  $l = 0.1$  cm, at 4 mm  $\rho$  has been equal to  $0.23 \angle -65.4^\circ$  for  $l = 0.4$  cm and at 2 mm,  $\rho$  has been equal to  $0.419 \angle 30.7^\circ$  for  $l = 0.4$  cm. With these values we have found for  $\alpha$  the attenuation factor as a function of the wavelength,

<u>Wavelength</u>	<u>Temperature</u>	$R =  \rho ^2$ <u>Reflection Coefficient</u>	<u><math>\alpha</math> (cm<sup>-1</sup>)</u>
8 mm	4.2°	0	2.23
4 mm	4.2°	0.056	9.83*
2 mm	4.2°	0.176	2.25

Table III. The absorption coefficient  $\alpha$  for different wavelengths as found experimentally.  
\* (The figure at 4 mm wavelength appears unusually high.)

### 3.0 THE SAMPLE DETECTOR

#### 3.1 Package Requirements

The physical container or package in which the detecting element must be housed is of considerable importance in this program since it must be compatible with the operating requirements of the detecting element. The operating environment necessary for the detecting element to achieve maximum detectivity is discussed earlier in this report, and a few of the more important items that affect the package design are discussed below.

One consideration that is of prime importance in designing the package is the end use consideration. In this program, Hall effect measurements had to be made to determine the relation between magnetic field and available energy levels in the different materials. It was desirable to make these measurements and evaluate most of this data before photoconductivity measurements were initiated. This consideration led to the conclusion that at least two packages were necessary so that Hall effect measurements could commence early in the program while plans were being formulated for the dewar for photoconductivity measurements. Another advantage of having the two dewars is that both types of measurements could be run simultaneously, if desired.

An important factor affecting the package configuration is the temperature at which the detecting material must be operated. Section 1.0 discusses this temperature requirement in detail and leads to the conclusion that the sample must be operated in the liquid helium temperature range. According to the present state of the art in cryogenics, liquid helium is best transported and stored in a nitrogen-shielded dewar configuration with high vacuum insulation. With this information in mind, two dewar packages have been made available - one a modification of an existing Raytheon-owned dewar for Hall measurements and a new dewar for photoconductivity measurements. Detector temperatures below the normal boiling point of liquid helium ( $4.2^{\circ}\text{K}$ ) can be attained by pumping over liquid helium, and provisions to operate the package at very low temperatures by this method have been included in the design. A plot of helium boiling point versus vapor pressure for  $\text{He}_4$  is shown in Figure 21.

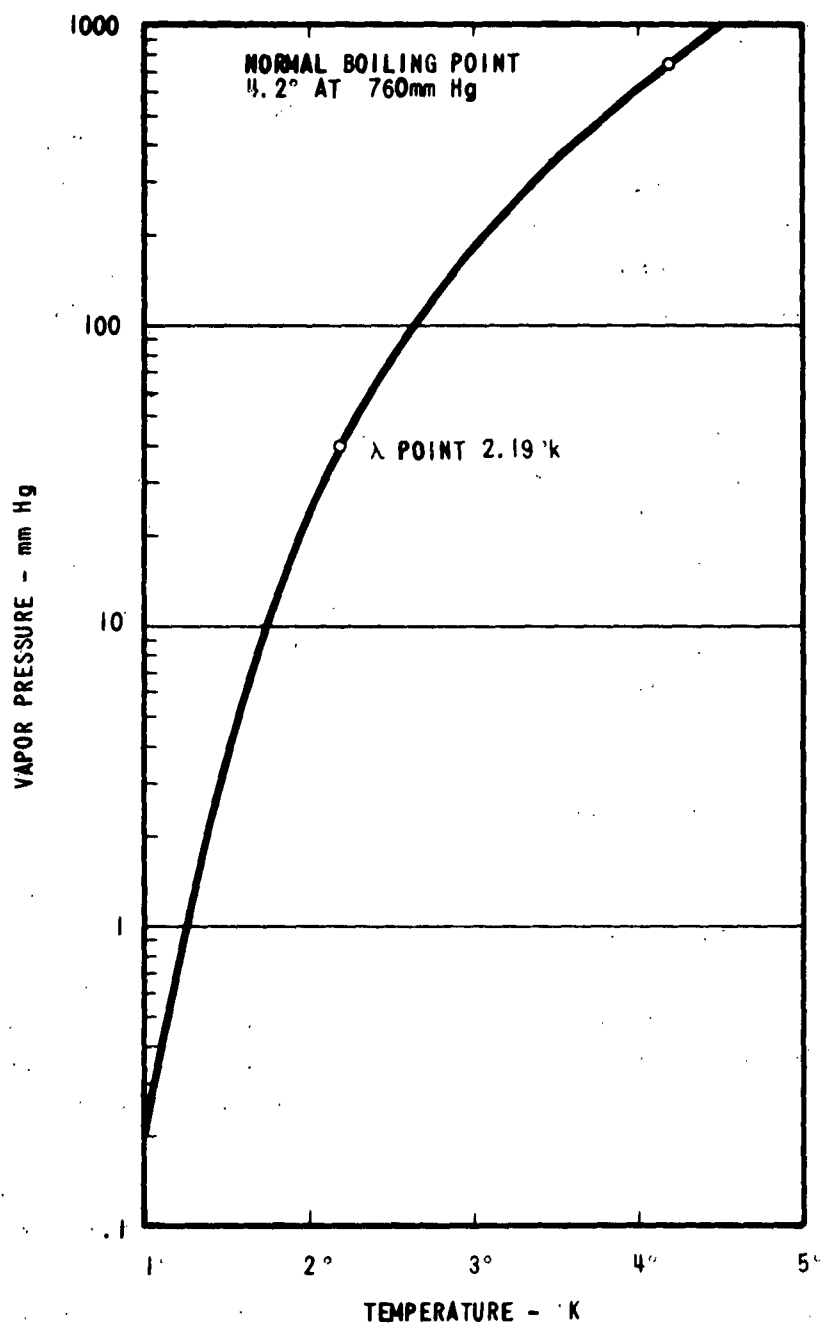


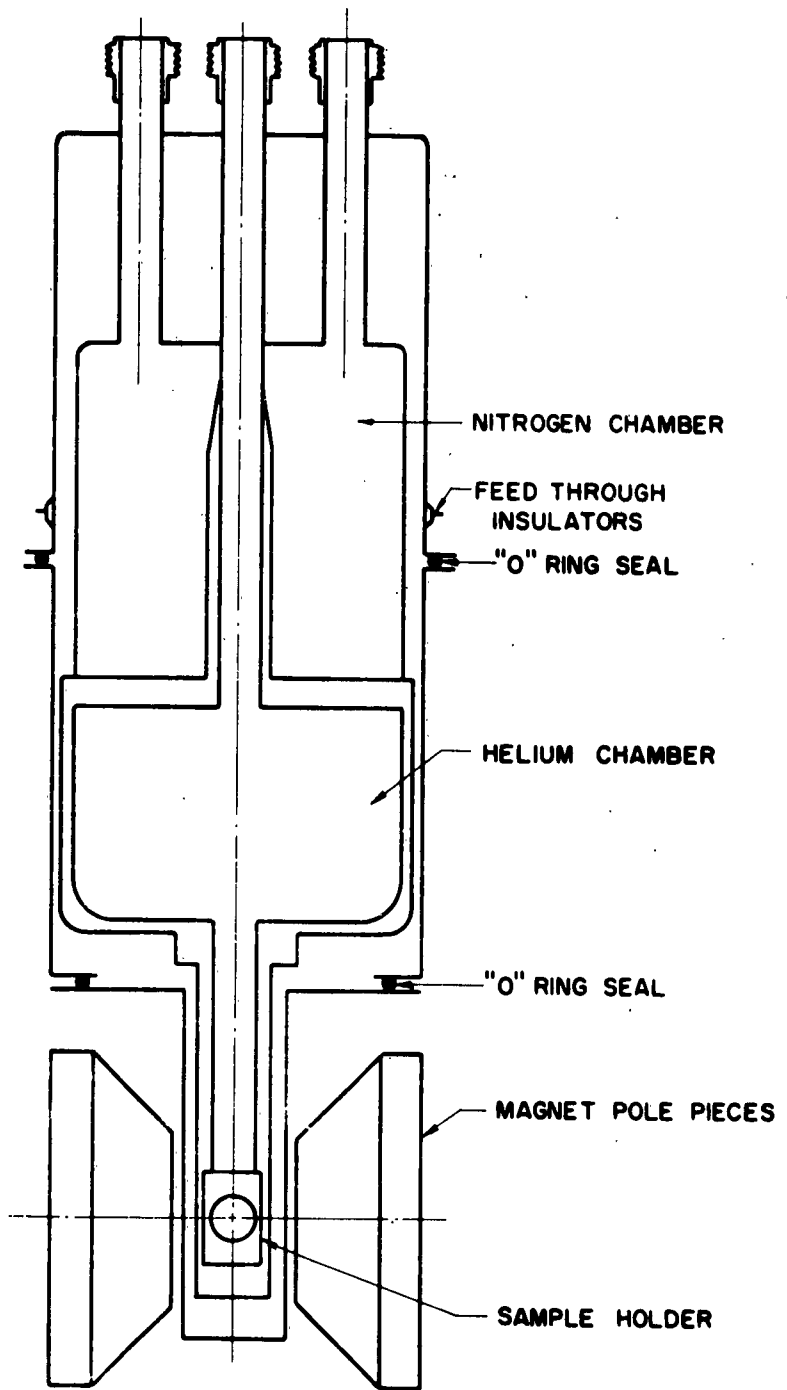
FIG.21 VAPOR PRESSURE - TEMPERATURE RELATIONSHIP FOR HELIUM

Another factor of importance that affects the package design is the necessity of providing a magnetic field. Variable field strengths are necessary for the Hall effect measurements and, based on Putley's prior work,<sup>11</sup> the application of a magnetic field also seemed necessary for maximum photoconductive response. For Hall measurements, magnetic field strengths up to 10,000 gauss are available from a 4" diameter magnet system which is installed in our laboratory. Due to its availability and flexibility, it was decided to adapt a package for Hall effect measurements with a "cold finger" and use it in conjunction with this magnet system. The photoconductivity measurements were done in a dewar with an integral superconducting solenoid, and the reasons for this combination are given later in this report.

Some of the other factors entering into the package design considerations are reduction of microphonics, provision for windows to allow the radiation to enter, optical filters, lead wires from the sample through the package wall, and, finally, the helium hold time of the completed unit.

#### Package for Hall Effect Measurements

As previously stated, since a variable field magnet system was immediately available in our laboratory, we decided to make use of this system for the Hall effect measurements part of this program. A dewar that would be compatible with this magnet system was necessary, and, since liquid helium dewar packages are currently being made in our department for use with our long wavelength detector line, it was convenient to modify one of these packages with a "cold finger" and use this between the pole pieces of the magnet system. An outline drawing of this package is shown in Figure 22 and photographs of the finished dewar ready for use are shown in Figures 3 and 23. During a test of this dewar to determine the extent of which the temperature of the semiconductor sample could be lowered, we observed that temperatures as low as 1.3°K could be maintained by pumping over the liquid helium.



**HALL EFFECT DEWAR FOR  
 FIGURE 22 MILLIMETER WAVE DETECTOR PROGRAM**

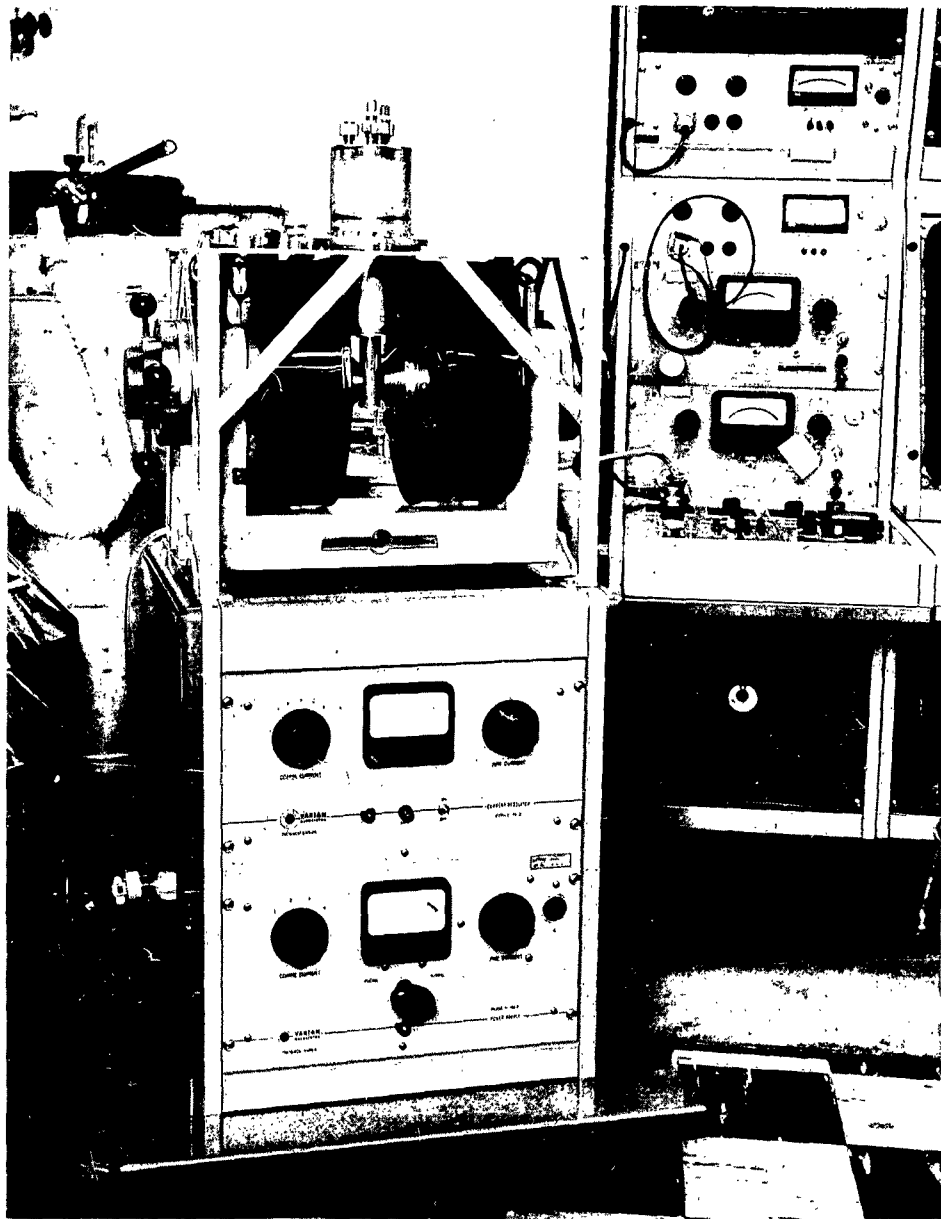


Figure 23. MAGNET AND ASSOCIATED EQUIPMENT  
FOR HALL EFFECT MEASUREMENTS

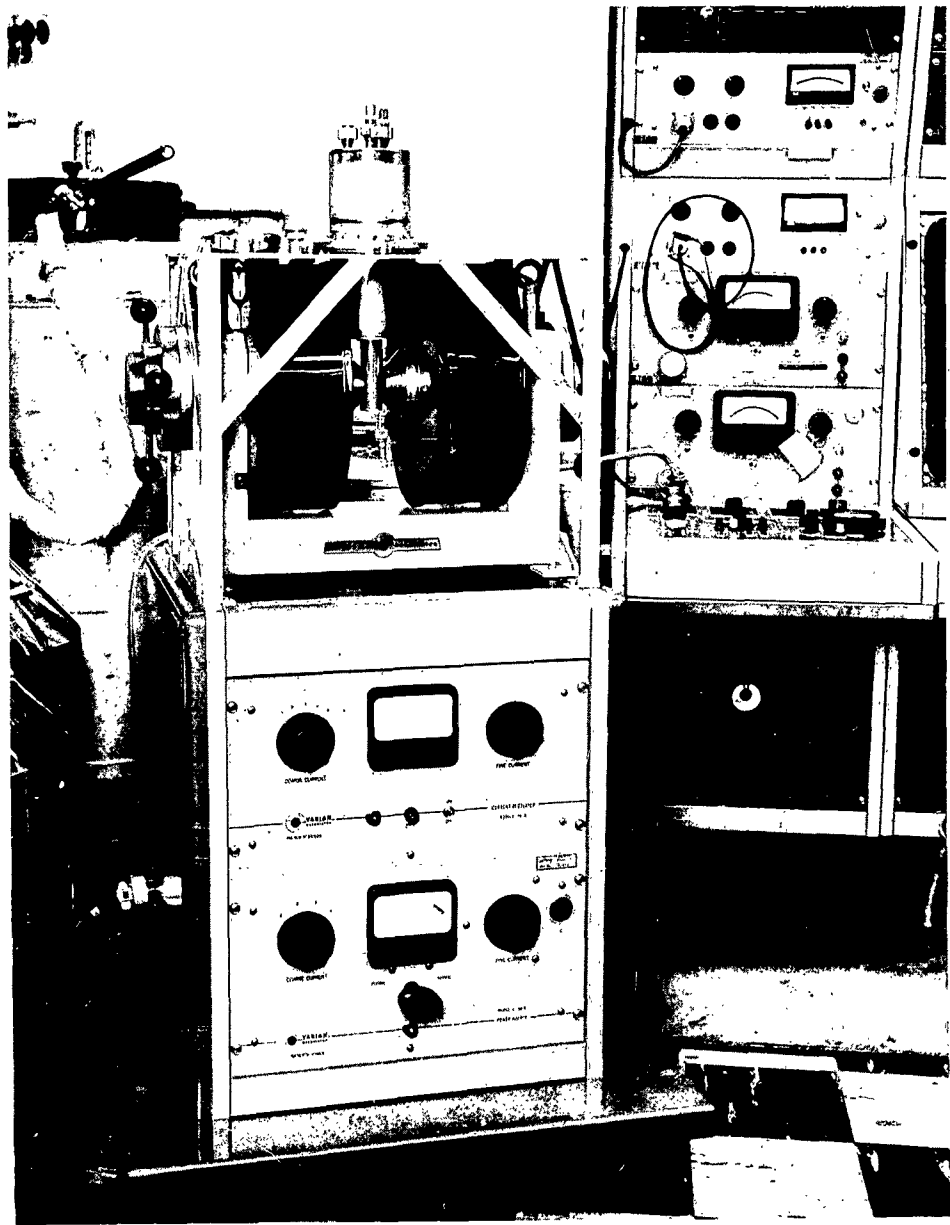


Figure 23. MAGNET AND ASSOCIATED EQUIPMENT  
FOR HALL EFFECT MEASUREMENTS

Some photoconductivity measurements were also made using this dewar. This was accomplished by fitting the outer vacuum wall of the "cold finger" with a window and mounting the sample on the inner "cold finger" in such a manner that the radiation could enter to the sample through the window. A filter was mounted over the sample so that room temperature background radiation impinging upon the sample would be reduced.

### Superconducting Solenoid

Generation of high magnetic field strengths by the use of superconducting solenoids is a development of the last few years. The breakthrough really came about when it was discovered that some alloys and compounds would remain superconductive at much higher field strengths and while carrying higher current densities than the elemental superconductors such as mercury, niobium and lead. The development of these materials is well covered in the literature so that only the application of these new superconducting materials to this program will be discussed here.

The considerations which prove the applicability of a superconducting solenoid to this program can best be shown by a short comparison of conventional and superconducting magnet systems.

It has been shown that superconducting solenoids can be operated with little or no power input in comparison to the large amounts of power that must be dissipated to operate a conventional magnet system.<sup>16</sup> However, the cost of refrigerating a solenoid to the required liquid helium temperature level and keeping it there negates some of the advantage gained by its low operating power requirement. The ideal situation for application of a superconducting solenoid is where low temperatures are already required for other reasons. Such is the case in our application where the detector element must be operated while being cooled to the liquid helium temperature range. The extra mass that must initially be cooled depends, of course, on the volume of the solenoid, but has, in this program, required an almost negligible increase in the amount of helium required to cool and fill the dewar itself. After filling, there is a slightly larger helium boiloff rate when the solenoid is installed due to the heat leak of the lead wire to the solenoid.

Of the newer superconducting alloys, some have inherent properties or have been developed further making them more desirable as solenoid windings than others. Many of the superconducting alloys are extremely brittle and do not lend themselves readily to use as solenoid windings. Niobium-zirconium, while not having the best superconducting properties of the alloys studied, does have a good combination of s. c. properties and mechanical workability which, at present, makes it the most promising alloy system to be considered for solenoid windings. Solenoids with field strengths of up to 68,000 gauss have been constructed using windings made from this alloy system.<sup>17</sup> The particular alloy of this system chosen for our application was a 75% niobium - 25% zirconium alloy which has a good combination of mechanical workability and high critical field while carrying an appreciable amount of current.

The insulation of the superconducting wire is accomplished by coating the wire with an epoxy coating which has been proven to be reliable at cryogenic temperatures. The wire was supplied to us by Westinghouse and was coated by them also. It is interesting to note that superconducting wire may also be insulated by covering it with a coating of a metal such as copper or nickel, since even these metals are insulators when compared to the superconductors.

### Solenoid Design

The first item to be decided when designing the solenoid itself is the maximum field strength desired at the center of the bore of the solenoid. In our case, it was felt that a central field of 10,000 gauss would be sufficient and that the field uniformity should be 5% within a 1/4 inch diameter sphere at the center of the field. Due to space requirements of the detector adapter, it was felt that the diameter of the bore of the windings should be 3/4 inch. Power supply considerations and size of the lead wires required, coupled with critical field versus critical current tests on the superconducting wire, indicated that this field should be attained at no more than 14 amperes current.

The maximum diameter and length of the solenoid are related to the above specifications by the following equation

$$H = \frac{G \sqrt{\gamma} I a_1}{A}$$

where  $G \sqrt{\gamma}$  = Geometric factors depending on dimensions of the solenoid

I = Current per turn in amperes

$a_1$  = Inside radius of windings

A = Cross sectional area allowed for one conductor wire.

Since all the other values are known, this equation can be solved for  $G \sqrt{\gamma}$ . After this value is calculated, the geometric ratio of solenoid length to outside diameter is manipulated until the field uniformity is within the desired range and the necessary value of  $G \sqrt{\gamma}$  is obtained. The calculated field uniformity and relative size factors which were arrived at for this application are shown in Figure 24.

The superconducting solenoid supplied on this program was wound with .010 in. dia. niobium-zirconium wire supplied by Westinghouse. The epoxy insulation makes the diameter of the coated wire .011 in., and 2242 turns have been wound to make this solenoid. The room temperature resistance of the coil is 1595 ohms. Other information pertinent to operating the solenoid is included in the operating instructions.

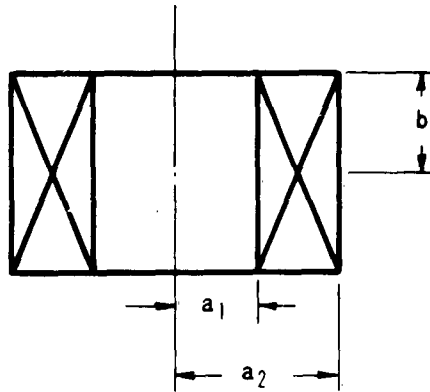
Although the only power necessary to operate a semiconductor solenoid from a power supply is that necessary to overcome the resistance of the lead wires, the main advantage of a superconducting solenoid is attained when the solenoid can be operated without the power supply connected. This operating condition is known as persistent operation and is accomplished by completing the circuit with a superconducting shunt. Figure 25 shows one arrangement by which persistent operation may be attained. The shunt is kept in the superconducting state during persistent operation by cooling it sufficiently, but, for conditions when it is desired to change the field, there must be a provision to allow the shunt to be made "normal" or resistive. This can be accomplished magnetically or thermally by exceeding either the critical field or the critical temperature of the wire. The

WINDING DIMENSIONS

$$\frac{3}{4} \text{ I.D.} = 2a_1$$

$$\frac{7}{8} \text{ LONG} = 2b$$

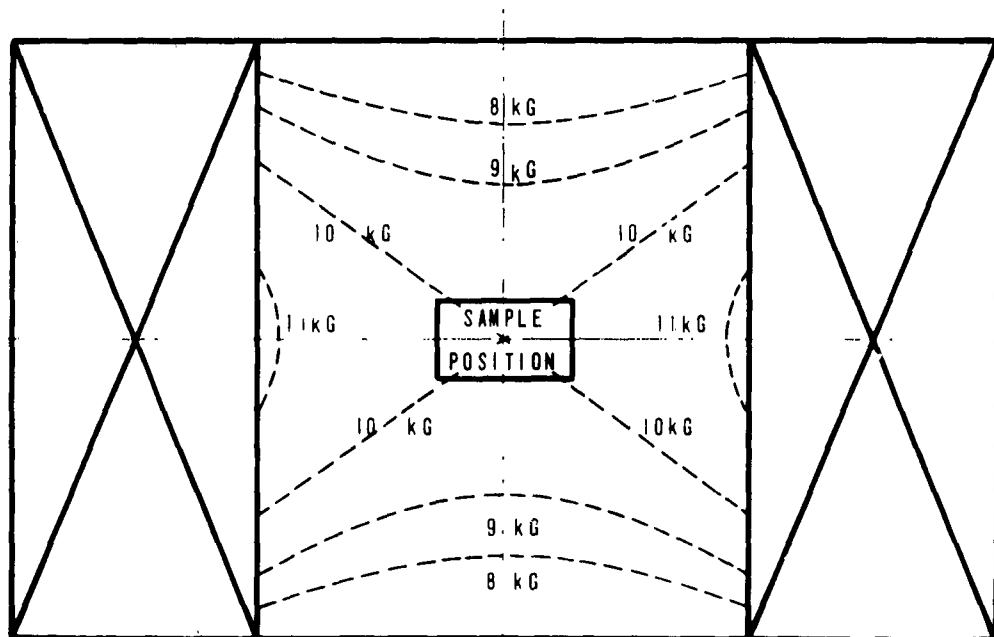
$$1 \frac{1}{2} \text{ O.D.} = 2a_2$$



$$\alpha = \frac{a_2}{a_1} = 2.05$$

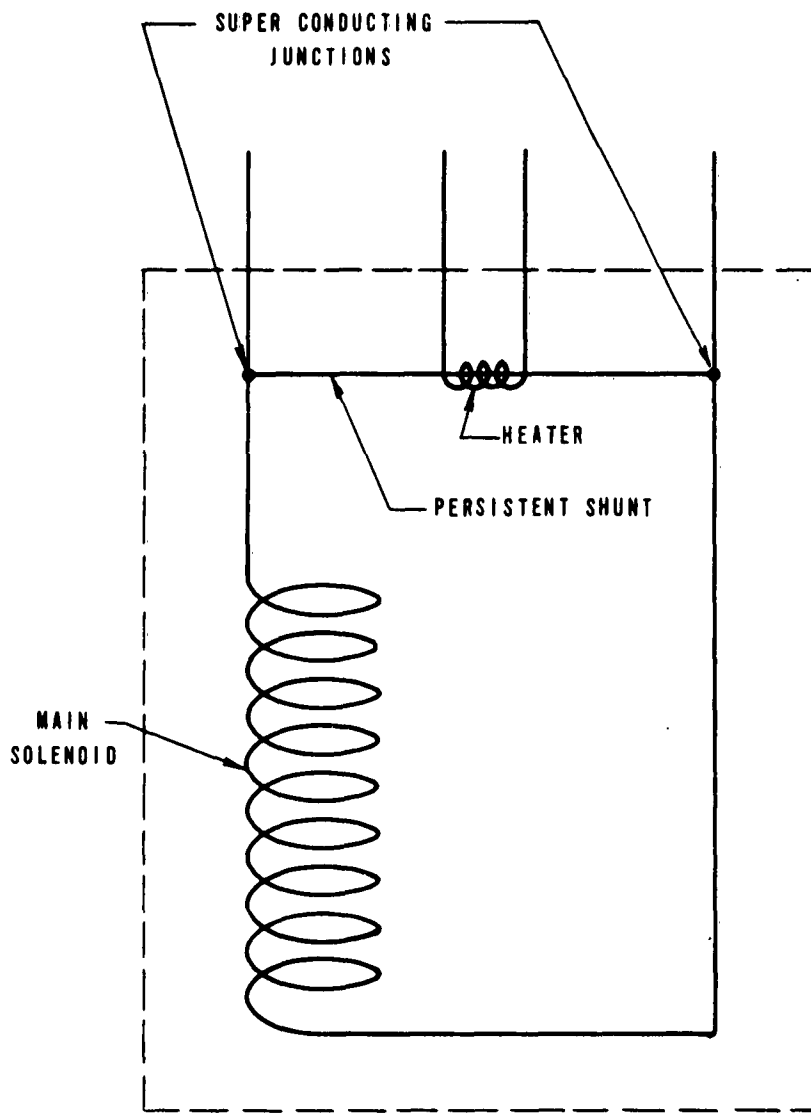
$$\beta = \frac{b}{a_1} = 1.18$$

FIELD DISTRIBUTION AT  $H_{O_2} = 10$  KILOGAUSS  
 SAMPLE SIZE: 5mm WIDE X 3mm THICK



SCALE: 4-1

FIGURE 24 SOLENOID DIMENSIONS AND FIELD DISTRIBUTION



NOTE: COMPONENTS WITHIN DOTTED LINE ARE AT  $\pm 4.2^{\circ}\text{K}$

FIGURE 25 SCHEMATIC OF SOLENOID CONNECTED FOR PERSISTENT OPERATION

shunt was quenched thermally in our application, and this was done by winding some heater wire around a short section of the shunting wire as shown in the figure. The procedure for operating the solenoid is to first apply enough current to the main solenoid windings to obtain the desired field strength. The shunt is then made normal by applying a voltage to the heater wire. After several seconds, the heater voltage may be shut off and, after giving the shunt enough time to be superconductive again, the power supply may then be disconnected and removed.

The power supply requirements for operating the superconducting solenoid are a direct current supply for the main solenoid current and either an ac or dc heater supply for operating the shunt. The dc supply should be capable of providing low ripple current up to 15 amperes and should be adjustable. For our testing we used an automobile-type six volt storage battery with a rheostat as shown in Figure 26. The shunt heater was controlled by a Variac run from a 110 volt ac line. More sophisticated rectifier type power supplies could, of course, be used, but we found that by recharging the storage cell over night we could run as many tests as desired without discharging the cell excessively.

#### Dewar-Solenoid Package for Photoconductivity Measurements

As originally proposed, the finished detector package to be delivered at the end of the program was designed with a superconducting solenoid built into the dewar package. As proposed the configuration of the dewar was such that this solenoid was to be conduction cooled as shown in Figure 27. The main advantage of conduction cooling the solenoid is that the solenoid is then in the vacuum space and is not subject to moisture damage or high thermal shock, a type of damage which is possible when the solenoid is immersed in the liquid helium. After construction of the dewar, the solenoid spindle was attached and the spindle temperature at the extreme lower end was measured while pumping over the liquid helium. The results of these tests showed that the temperature differential from the boiling helium to the far end of the spindle was only .2 - .4°K, and temperatures as low as 1.5°K were measured on this end of the spindle. However, after the

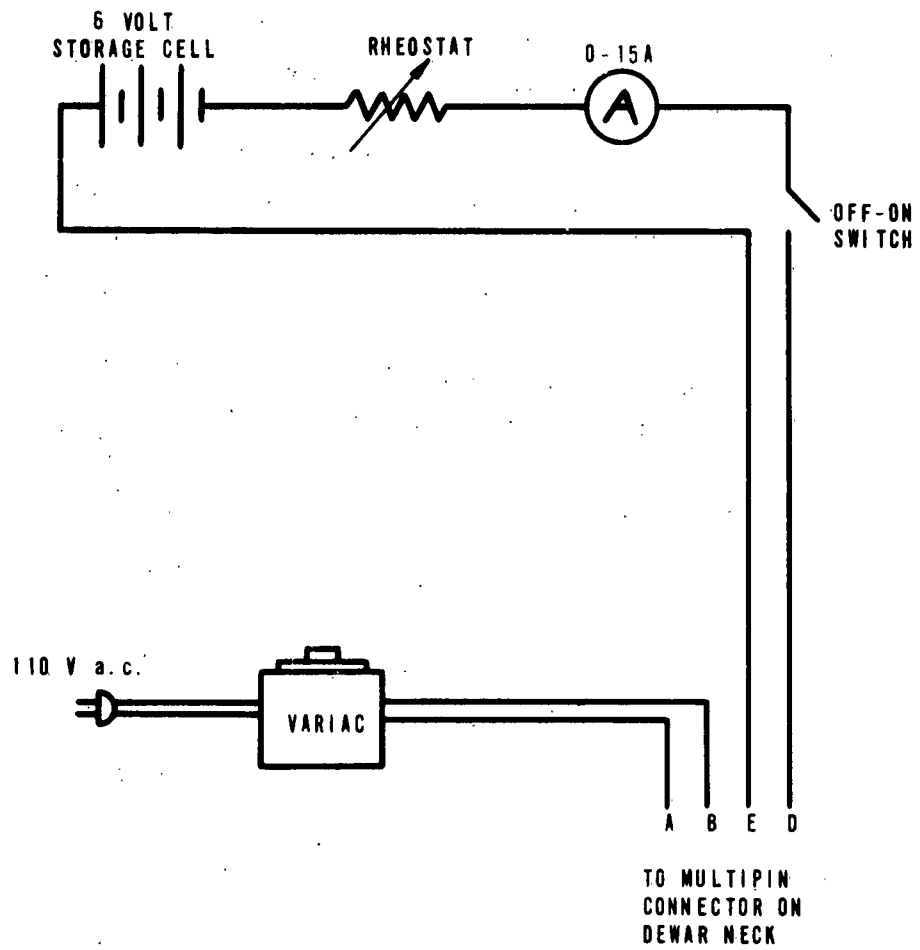


FIGURE 26

SUPERCONDUCTING SOLENOID  
POWER SUPPLY SCHEMATIC

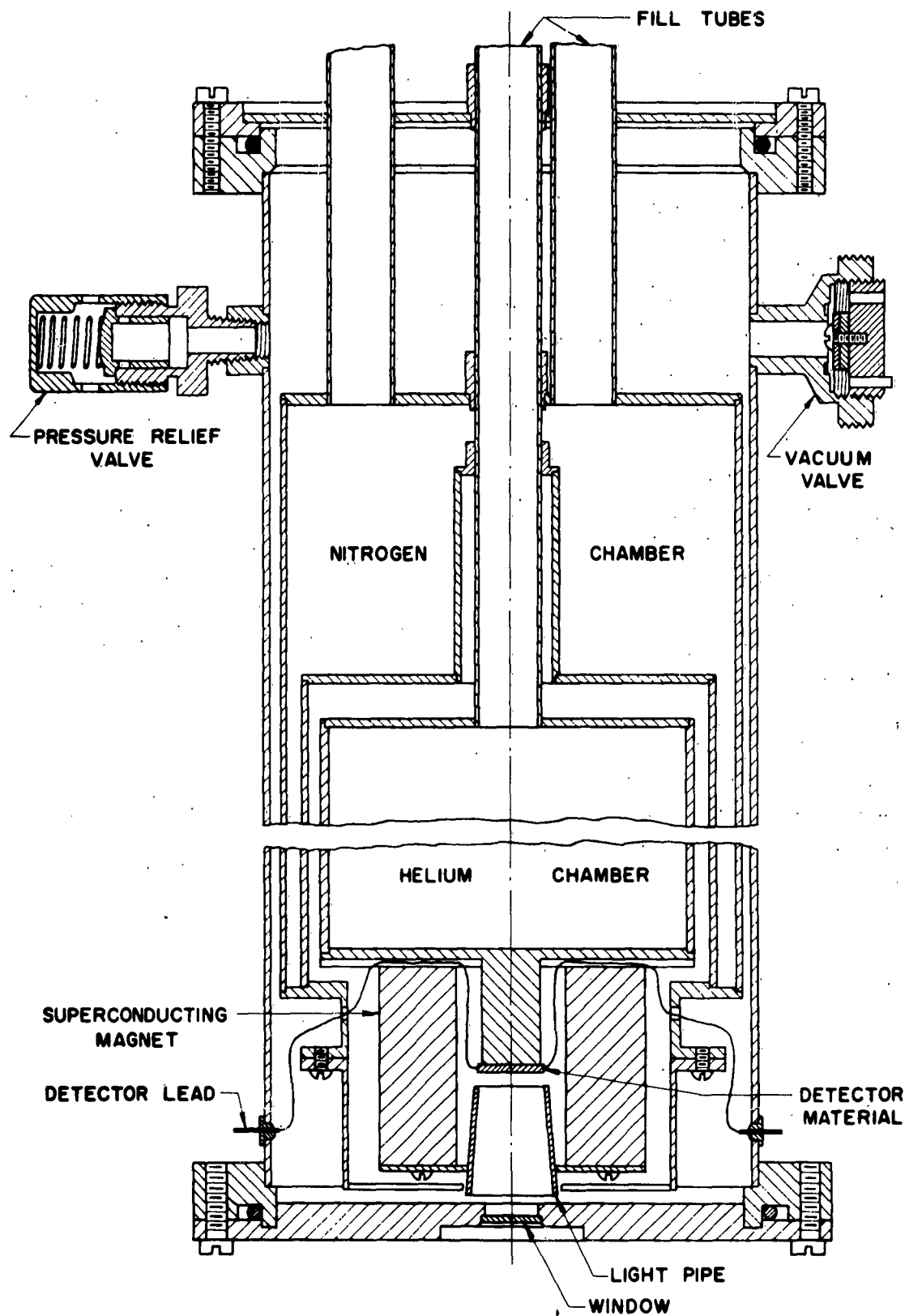


FIGURE 27 HELIUM DEWAR MODIFICATION FOR PHOTOCONDUCTIVE MILLIMETER WAVE DETECTOR

solenoid was wound and attached to the dewar and operation was attempted, it was found that the solenoid would become normal at very low field strengths. The problem was eventually traced to Joule heating of the lead wires when the current is applied. This heating causes the windings to go normal progressively from the junctions where the lead wires are connected to the superconducting wires. Attempts to cool the junctions by conduction improved the situation somewhat, and a field strength of 5000 gauss has been generated with this configuration. This is only 1/2 of the design field of the solenoid, and, since it was known that the solenoid would operate at the design field strength while submerged in liquid helium, we decided to follow this other approach while there was still time in the program.

Another alternate solution was weighed, and that was to conduction cool the solenoid itself and bring the lead wires through the bottom of the helium chamber so that the troublesome junctions would be immersed in the liquid helium. This would require that a vacuum tight insulator assembly be built into the helium chamber bottom, and, since insulator assemblies of this type are not reliable under conditions of thermal shock such as would occur when the dewar was filled with liquid helium, it was decided not to work on this solution.

A dewar package in which the superconducting solenoid could be submerged in liquid helium was then designed and constructed, and an outline drawing of this dewar is shown in Figure 28. The detector material is mounted in vacuum at the center of the field of the solenoid on an adapter which is removable from the dewar. The construction of this end of the package was shown more clearly in Figure 14. Tests on the solenoid while run in this package show that the solenoid will generate fields at least 10% over the design field strength of 10,000 gauss. Test results of the unit as a millimeter wave detector are reported elsewhere in this report.

With this configuration, the solenoid may be removed without disturbing the insulating vacuum of the dewar.

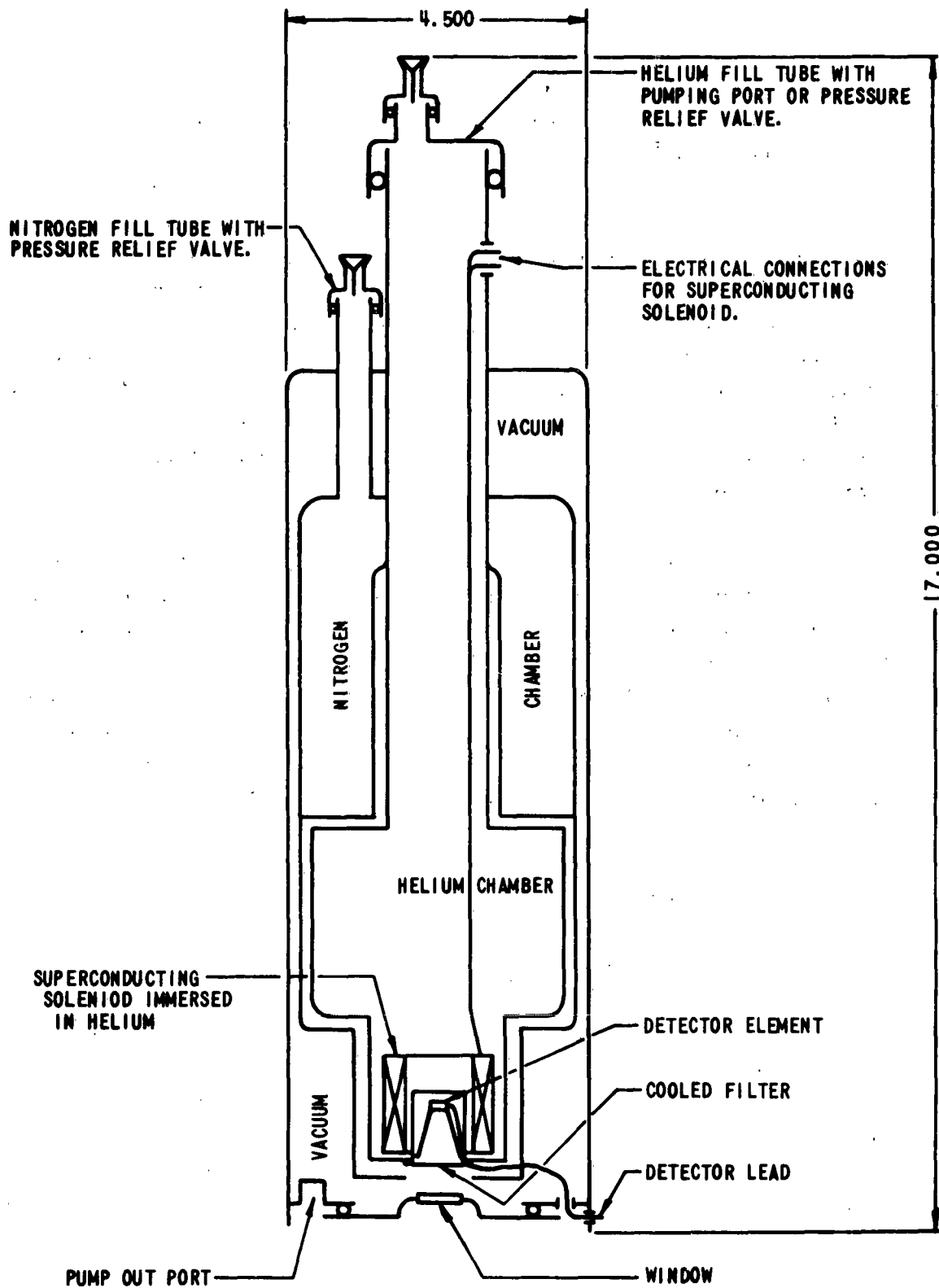


FIGURE 28 HALF SIZE OUTLINE DRAWING OF PHOTOELECTRIC MILLIMETER WAVE DETECTOR

A problem was encountered while attempting to run the solenoid persistent at the design fields. With the shunt connected, the field strength could not be increased to the design field without going normal. This problem was traced to the making of superconducting joints in the shunt connections. These junctions must remain superconductive while carrying the desired operating current. There are several methods of making these junctions - soldering, welding, and the use of compression joints. Of these methods, compression joints, where the wires are merely squeezed together, appears to be the most promising method and a modification of this technique yielded a joint which would allow the solenoid to operate persistently at the design field. However, some residual resistance is still present in the joints, and, when operated persistently, there is some field strength decay with time.

The procedure for persistent operation is to increase the amperage to the desired field level. In the case of the solenoid supplied on this contract, the ratio is 750 gauss per ampere. When the desired field is attained, the persistent switch should be supplied with 17 volts ac and then shut off. The power supply may now be disconnected and the solenoid will operate persistently. To operate continuously at a particular field strength, the persistent shunt must be disconnected and the solenoid is then operated similar to any other solenoid. No more than 15 amperes should be applied to the coil to avoid burning out the lead wires.

### 3.2 Operating Instructions

#### 3.2.1 Evacuating the Dewar

The dewar may be evacuated when desired, by using the removable valve handle supplied with the dewar, in the following manner. The valve handle is first threaded into the evacuation port on the window end of the dewar and then connected to a high vacuum system (a liquid nitrogen trapped diffusion pump or an ionic pump). After the vacuum line is pumped out, the dewar valve may be opened by simultaneously pushing in and turning the handle of the vacuum valve

until it engages with the valve seat. The valve is fully opened by turning the handle counterclockwise until it stops (about 2 turns). The handle should then be pulled out about 1/2" to reduce the flow friction in the valve handle. Heat may be applied to the dewar to aid outgassing during evacuation, but the dewar temperature should not exceed 100°C.

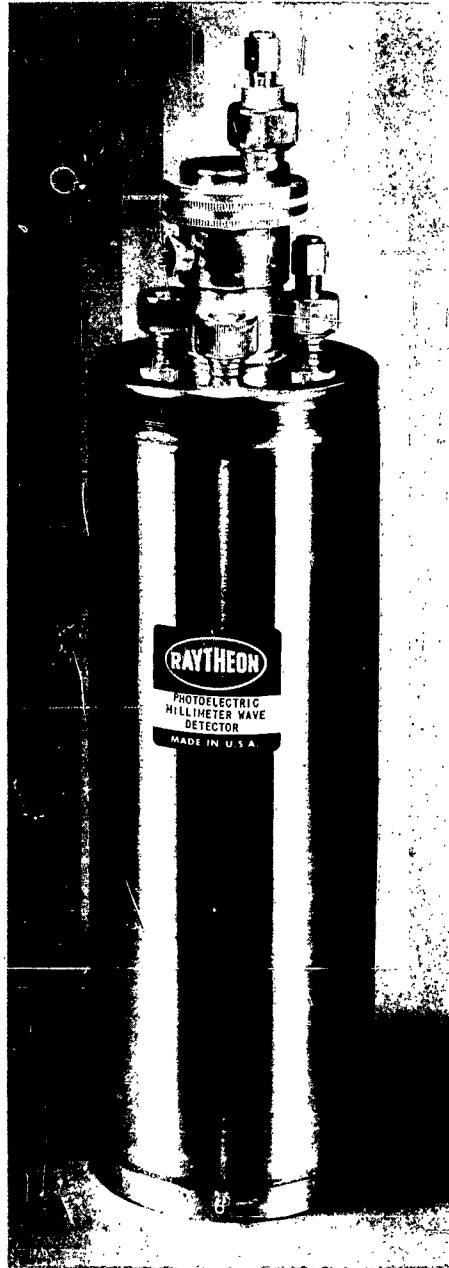
After the dewar is evacuated to the desired level ( $10^{-5}$  mm Hg or better), the valve may be closed by pushing in the handle until it engages the seat and then turning the handle clockwise until the valve seats. (When seating the valve, do not apply a torque of over ten inch-pounds or the sealing washer will be damaged.) The valve is then removed by pulling the valve handle out about 1/2" and disconnecting the vacuum line. The handle may then be removed by unscrewing it from the evacuation port of the dewar.

#### Cooling Procedure

If not familiar with the handling of liquified gases, it is recommended to read the handling precautions printed and distributed by the gas manufacturers before attempting to operate the detector. The dewar is cooled by first filling the nitrogen compartment with liquid nitrogen. This is easily accomplished by removing the caps from all of the nitrogen fill tubes (see Figure 29) and by using a small polyethylene funnel in one of the tubes for filling and using the other two tubes for vents. (Note: If the outer shell of the dewar should become frosted below the upper weld joint, the insulating vacuum is poor and the dewar should be warmed up and repumped.) The dewar should be in the position shown in the figure during filling.

After the nitrogen compartment is filled, the inner helium compartment may be filled. To conserve expensive helium, it is desirable to precool the helium chamber to liquid nitrogen temperature. This can be accomplished either by allowing the dewar to stand until the inner compartment comes to equilibrium temperature with the surrounding cold nitrogen compartment, which takes approximately one-half hour, or by pouring some nitrogen in the helium

Helium Fill Tube



Nitrogen Fill Tubes

Figure 29. PHOTOELECTRIC MILLIMETER WAVE DETECTOR

compartment. If the latter precooling method is used, care must be taken to pour out all the nitrogen before helium is added or else the helium will freeze the nitrogen and possibly cause blockage in the neck of the dewar which could cause the dewar to rupture.

Helium must be transferred to the dewar through a vacuum insulated transfer tube, and the end that goes into the detector dewar must not be larger than 3/8" diameter to allow for room for the gas to escape. Experience with the transfer equipment is necessary to determine visually when the dewar is filled with helium, but one way to be sure is to weigh the dewar before and after transfer. It should be possible to fill the dewar with 350 - 400 cc of helium and this corresponds to an increase in dewar weight of 40 - 50 gms.

After filling, the pressure relief caps should be replaced on the fill tubes so that the gas evaporating from the liquid will be safely exhausted to the atmosphere and also so that no water vapor from the air will migrate down the fill tube and freeze out on the walls, since, again, this could cause blockage and dewar rupture. During operation, the dewar should not be tilted at an angle of over 45 degrees from that shown in Figure 29 or excessive liquid boiloff will be experienced.

If it is desired to lower the detector temperature by pumping over the liquid helium, a pressure regulating device such as a manostat should be installed between the vacuum pump and the dewar. A pressure relief valve should be installed in the line close to the dewar to avoid pressure increase in case the pump should unintentionally be shut off.

#### Operating the Solenoid

After the dewar is properly evacuated and cooled with helium, the solenoid may be operated. If there is liquid helium in the helium chamber, it can safely be assumed that the solenoid is in the superconducting state, but, in order to check this, the solenoid resistance may be measured across pins D and E on the dewar neck. The measured resistance will be below .2 ohm if the

solenoid is superconducting. (This resistance is actually the resistance of the lead wires from the pins to the solenoid.) The room temperature resistance of the solenoid is 1595 ohms, and, at nitrogen temperature, the resistance drops to approximately 1000 ohms.

When superconducting, the solenoid can be energized from a power supply such as is shown in Figure 26. If desired, a low ripple dc power supply can be used in place of the battery-rheostat combination, but the supply should not be of the constant current type to avoid burning out the solenoid if it goes normal.

As delivered, the solenoid is wired for persistent operation, and the solenoid wiring schematic of the dewar is shown in Figure 25. The field is established in the solenoid by supplying current to pins D and E on the dewar neck at the rate of one ampere for every 750 gauss, and, when the current corresponding to the desired field is applied, the superconducting shunt is made normal by supplying pins A and B with 17 volts ac either from a Variac or from a stepdown transformer. This causes the current to flow through the solenoid instead of the shunt and the field is then established. When the battery solenoid supply is used, a slight dip in current can be observed on the meter when the field is established in the solenoid. After this current dip is observed, the voltage to the superconducting shunt may be shut off and then the solenoid power supply can be shut off and removed.

To shut off the field, the shunt is made normal and the field immediately collapses.

If the current is increased too fast or if the liquid helium level is low, the solenoid may go normal and the solenoid current will not increase with voltage. It has been our experience that when operated from a constant voltage power supply, such as a battery, it does the solenoid no harm to go normal, but the solenoid current should be then shut off to allow the solenoid to return to the superconductive state.

The solenoid may be operated from a power supply without the persistent arrangement by disconnecting the superconducting shunt. This requires that the solenoid be removed from the dewar and disconnected. Since special tools are required to remove the solenoid, the detector should be returned to Raytheon for this modification.

#### Operating the Detector

Complete information on optimum magnetic field and optimum biasing current versus detectivity of this detector are given elsewhere in the report and before operating the detector it would be advantageous to refer to Section 2 for detailed information. In general, the optimum biasing current was in the 80-100  $\mu\text{A}$  range, and this was applied as shown in Figure 13, which also shows the schematic of the other test equipment. The optimum load resistor was found to be 100 K ohm.

The millimeter radiation incident on the detector should be chopped at a frequency which can be tuned to easily by the preamplifier. The output from the preamplifier can then be read out on a tuned voltmeter such as a General Radio Model 1554A Sound and Vibration Analyzer.

#### Window Adapter Removal

The window assembly is sealed to the rest of the dewar by using an "O" ring and four screws. This window assembly may be removed to change the window material or to work on the detector. The procedure starts with "breaking" the vacuum in the dewar. This is accomplished by opening the evacuation valve and allowing the dewar to fill with dry air or a dry gas such as nitrogen. The window adapter may then be removed by removing the four screws from the face of the window assembly and then removing it. The window may be replaced by reversing the procedure outlined above.

Note: Since water vapor is difficult to remove from the vacuum space, the window assembly should not be removed while the dewar is cold.

## REFERENCES

1. S. J. Fray and J. F. C. Oliver, *J. Sci. Inst.* 36, 195 (1959).
2. Final Report, "Long Wavelength Infrared Detector Research and Components Measurement", Part I, Raytheon Company, Research Division, Contract No. AF33(616)-7983 (Classified Confidential).
3. B. V. Rollin and A. D. Petford, *J. Electronics and Control*, 2, 171 (1955).
4. C. S. Hung, *Phys. Rev.* 79, 727 (1950).
5. C. S. Hung and J. R. Gliessman, *Phys. Rev.* 79, 726 (1950); 96, 1226 (1954).
6. H. Fritzsche and K. Lark-Horowitz, *Physica* 20, 834 (1954).
7. Y. Yafet, R. W. Keyes and E. Adams, *J. Phys. Chem. Solids*, 1, 137 (1956).
8. R. W. Keyes and R. J. Sladek, *J. Phys. Chem. Solids*, 1, 143 (1956).
9. R. J. Sladek, *J. Phys. Chem. Solids*, 5, 157 (1958).
10. E. H. Putley, *Proc. Phys. Soc.* 76, 802 (1960).
11. E. H. Putley, *J. Phys. Chem. Solids*, 22, 241 (1961).
12. W. Shockley, "Electrons and Holes in Semiconductors", Chapt. 11, D. Van Nostrand Company, Inc., New York (1950).
13. E. H. Putley, "The Hall Effect and Related Phenomena", Butterworths and Company, Washington, D. C., (1960) Section 2.6.
14. See Reference 12, p. 211.
15. E. H. Putley, *Proc. Phys. Soc. Lond.* 73, 280 (1959).
16. R. W. Boom, R. S. Livingston, Superconducting Solenoids, *Proc. I.R.E.* 50, 3, p. 274, March 1962.
17. H. Riemersma, et al. A Variable Composition, High Field Superconducting Solenoid, *J. Appl. Phys.* 33, 12, 3499-3504, Dec. 1962.

DISTRIBUTION LIST FOR CONTRACT REPORTS

	<u>Nr of Copies</u>
RADC (RALTM, ATTN: Mr. LoMascolo) Griffiss AFB NY	3
RADC (RAAPT) Griffiss AFB NY	1
RADC (RAALD) Griffiss AFB NY	1
GEEIA (ROZMCAT) Griffiss AFB NY	1
RADC (RAIS, ATTN: Mr. Malloy) Griffiss AFB NY	1
US Army Electronics R and D Labs Liaison Officer RADC Griffiss AFB NY	1
AUL (3T) Maxwell AFB Ala	1
ASD (ASAPRD) Wright-Patterson AFB Ohio	1
Chief, Naval Research Lab ATTN: Code 2027 Wash 25 DC	1
Commanding Officer US Army Electronics R and D Labs ATTN: SELRA/SL-ADT Ft Monmouth NJ	1
AFSC (SCSE) Andrews AFB Wash 25 DC	1
ASTIA (TISIA-2) Arlington Hall Station Arlington 12 Va	10
RTD (RTGS) Bolling AFB Wash 25 DC	1

	<u>Nr. of Copies</u>
Electronic Communications, Inc. ATTN: Dr. J. Wiltse 1830 York Road Timonium, Md.	1
RADC (RAWED/Mr. R. Davis) Griffiss AFB NY	1
Commanding Officer USAERDL ATTN: SELRA/SL-PEE/Mr. N. Lipetz Ft Monmouth NJ	1
Bureau of Ships ATTN: Mr. L. W. Gumina Electronic Division Wash 25 DC	1
University of Illinois ATTN: Dr. P. V. Coleman College of Engineering Urbana, Ill.	1
Commander ASD (ASRNCF-1/Ferrite Section) Wright-Patterson AFB Ohio	1
Polytechnic Institute of Brooklyn ATTN: Dr. A. A. Oliner Microwave Research Institute 55 Johnson St. Brooklyn, NY	1
Sperry Microwave Co. ATTN: R. Duncan Clearwater, Fla.	1
Microwave Associates ATTN: Librarian Burlington, Mass.	1
AFCRL/Mr. F. J. Tucker Electromagnetic Radiation Lab Bedford, Mass.	1

	<u>Nr. of Copies</u>
NASA ATTN: Dr. Robert Coates, Code 520.1 Goddard Space Flight Center Greenbelt, Md.	1
Director Ballistic Research Lab Aberdeen Proving Ground Aberdeen, Md.	1
Aerospace Corp ATTN: Dr. R. C. Hansen Electronics Lab PO Box 95085 Los Angeles 25, Calif.	1
MIT, Lincoln Labs ATTN: Mr. G. Catuna Lexington 73, Mass.	1
The Martin Co. ATTN: Dr. Vernon C. Derr Orlando, Florida	1
Lawrence Radiation Lab ATTN: Mr. Charles B. Whanton University of Calif. PO Box 808 Livermore, Calif.	1
AGED ATTN: Mr. W. Kramer 346 Broadway, 8th Floor New York, New York	3
Boulder Lab ATTN: Dr. J. M. Richardson National Bureau of Standards Boulder, Colo.	1
USASRD ATTN: Mr. Leonard Hatkin Chief, Antenna and Microwave Circuitry Section Belmar, NJ	1
The Johns Hopkins University Dept of Electrical Engineering ATTN: Dr. Harvey Palmer Baltimore 18, Md.	1

	<u>Nr. of Copies</u>
MIT ATTN: Dr. Alan H. Barrett Room 26-459 Cambridge, Mass.	1
US Army Electronics R and D Labs ATTN: Dr. G. Gaubau Ft. Monmouth, NJ	1
Columbia University ATTN: Dr. S. P. Schlesinger Dept of Electrical Engineering New York 27, New York	1
University of Illinois ATTN: Prof. Paul E. Mayes Dept of Electrical Engineering 212 Elec. Engr. Research Lab Urbana, Ill.	1